TECHNICAL MEMORANDUM

395

CMOD5
An improved geophysical model function for ERS C-band scatterometry

Hans Hersbach

Research Department

January 2003

European Centre for Medium-Range Weather Forecasts
Europäisches Zentrum für mittelfristige Wettervorhersage
Centre européen pour les prévisions météorologiques à moyen terme

For additional copies please contact

The Library
ECMWF
Shinfield Park
Reading
RG2 9AX
library@ecmwf.int

Series: ECMWF Technical Memoranda

A full list of ECMWF Publications can be found on our web site under:
http://www.ecmwf.int/publications/

Abstract

A new geophysical model function (GMF) for the C-band scatterometers aboard the European Remote Sensing Satellites (ERS-1 and ERS-2) is presented. A GMF relates surface winds to a scatterometer backscatter signal from capillary waves at the ocean surface. From triplets of observed backscatter measurements, inversion of a GMF allows for the estimation of the 10m-wind vector.

The new GMF, CMOD5, was determined on the basis of a collocation between ERS-2 scatterometer backscatter triplets and ECMWF first-guess winds. The period between 1 August and 31 December 1998 was considered, embracing more than 22,000,000 collocations. In addition to this data set, recent results from experiments performed at high-wind conditions, were taken into account as well. As an extra constraint the position of the 2-dimensional CMOD5 surface (cone) in three-dimensional backscatter space was optimized with respect to observed triplets. Starting point was a prototype of CMOD5 developed at the Royal Netherlands Meteorological Institute (KNMI). However, its functional form was redesigned from scratch. CMOD5 is specified by 28 coefficients.

Compared to both CMOD4 (the GMF on which the ERS wind product is based since 1993) and the prototype CMOD5, CMOD5 shows an improved performance. Compared to the ECMWF first-guess winds, biases were reduced considerably for all incidence angles. For low incidence angles standard deviations were reduced as well, and the scatter index (standard deviation normalized by average wind speeds) was improved for the entire incidence-angle range. In the strong-wind sector, CMOD5 removes the under-estimation of CMOD4 winds. In general, the CMOD5 cone gives the best representation of the data cloud, especially for high winds. For low winds at high incidence angles, an asymmetry between the three ERS-2 beams was observed. Only for this sector, CMOD5 is not optimal because it assumes that the beams do behave identically.

1 Introduction

Since the launch of the ERS-1 platform in July 1991, surface wind-vector observations derived from space-borne scatterometer measurements have been available over the global oceans. In addition to the scatterometer on ERS-1 (operational until 1996 and functioning until December 1999), the continuity of this type of data flow was guaranteed by its successor on ERS-2 (scatterometer operational between 1995 and 2000), the NSCAT instrument on ADEOS-1 (September 1996 to June 1997), and the SeaWinds scatterometer on QuikSCAT (from 1999 onwards). In the near future, the re-dissemination of ERS-2 scatterometer data (January 2003), the launch of the ADEOS-2 satellite containing a SeaWinds instrument (December 2002), and the launch of METOP-2 (July 2005) containing the ASCAT instrument, should ensure continuity.

Not seldom space-borne observations are in data void areas, and, therefore, provide important information on the local state of the atmosphere. Scatterometer data has been used in the ECMWF assimilation system since January 1996. Although it only provides near-surface observations, the 4D-Var system at ECMWF (Rabier *et al.* 2000) is capable of transporting this information throughout the whole vertical. Examples are given by Isaksen (1997) and Leidner *et al.* (2003). Besides enhancing the ECMWF forecast system in general, scatterometer data has a beneficial effect on the analysis of tropical cyclones (see e.g., Tomassini *et al.* 1998, Isaksen and Stoffelen 2000, Leidner *et al.* 2003).

A scatterometer is an active microwave instrument which measures the normalized radar cross section (NRCS), from now on called backscatter, from the ocean surface. The intensity of this return signal is a measure of the wave height of capillary waves traveling in the direction of the emitted wave, which themselves are almost instantaneously generated by the local surface wind. The instrument is sensitive to a wave-length range that depends on the frequency of the emitted wave and its angle of incidence with respect to the normal to the ocean surface. For the ERS scatterometers, using a C-band frequency (5.3 GHz) and incidence angles between 20 and 60 degrees, the sensitive wavelength range is between 4 and 10 cm. Backscatter also depends on the

polarization of the emitted wave and the component of polarization of the returned signal measured by the instrument (both vertically for the ERS scatterometers).

As the scatterometer is most sensitive to capillary waves traveling in the look direction, the backscatter depends on the azimuth angle under which the observation is performed. Usually maximum backscatter is obtained when the incoming wave is aligned with the surface wind direction, and minimum backscatter when it is perpendicular to it. Therefore, by combining several measurements at different azimuth angles this upwind-crosswind effect not only allows for an estimate of the local surface wind speed, but, apart from a 180 degrees ambiguity, also for its direction. This is exactly the principle that is used by scatterometers. For ERS, for instance, three beams (fore, mid and aft) illuminate the same area, each under a different look angle. The Seawinds instrument on QuikSCAT combines up to four measurements to determine the 10m-wind vector. There is a difference in backscatter between a measurement in the upwind and downwind direction as well. This asymmetry allows, in principle, for the removal of the ambiguity in wind direction. However, the upwind-downwind differences are quite small and, therefore, in practice, it is difficult to decide which of the two solutions is the proper one.

A model that takes the above mentioned dependencies on backscatter into account is called a geophysical model function (GMF, or simply model function). There has been quite some theoretical work on the understanding of both the interaction of electro-magnetic waves with the sea surface (for which the principle mechanism is Bragg scattering) and the generation of capillary waves by the local surface stress or wind speed. The range of applicability and required accuracy of such theory-based GMF's is in general limited (an exception is the VIERS model, Janssen *et al.* 1998). For practical use, the relation between backscatter and wind speed still relies on empirical models. Examples are the CMOD models (Attema 1986, Cavanié and Offiler 1986, Stoffelen and Anderson 1997a, 1997b) for VV-polarized C-band scatterometry (ERS), and the NSCAT and QSCAT models for Ku-band scatterometry (e.g., Wentz and Smith 1999). These empirical models are based on collocation studies between scatterometer data (usually airborne) with in situ data or model fields. For instance, the ERS-1 prelaunch CMOD1 model function was deduced from several airborne campaigns performed in the 1980s. CMOD4 relied on a comparison between (space-borne) ERS-1 data and ECMWF analysis winds for a period in 1991 (Stoffelen and Anderson, 1997a, 1997b).

Since 24 February 1993, the operational ERS scatterometer wind product provided by ESA is based on CMOD4. The wind product is determined by minimizing a cost function expressing the misfit between an observed triplet of backscatter measurements and modeled (CMOD4) backscatter. Visualized in three-dimensional observation space, CMOD4 describes a two-dimensional cone (its parameters are wind speed and direction). The direction along the cone is sensitive to wind speed, the direction around the cone to wind direction. The cone has a double periodic structure: going from a wind direction from 0 to 360 degrees, it winds twice. The upwind-downwind asymmetry is the cause that both structures do not overlap. The diameter of the cone, finally, is determined by the size of the upwind-crosswind difference. The inverted wind vector is that solution on the cone that is closest to the observed triplet. A large distance of the triplet to this point on the cone (basically equal to the residual cost) indicates a low-quality observation and/or a deficiency of the GMF.

The CMOD4 inverted ERS winds perform within ESA's original instrument specifications, i.e., an average rms less than 2 $\mathrm{m\,s^{-1}}$ and an average bias less than 0.5 $\mathrm{m\,s^{-1}}$, when compared to operational global NWP wind fields. Within these margins, biases of CMOD4 winds are known to exist. For instance, in the low and medium wind-speed range, a wind-speed dependent bias has been observed from a triple collocation study with buoy winds and NCEP model winds (Stoffelen 1998). For the high wind speed sector, CMOD4 is known to overestimate backscatter, which, after inversion, results into too low winds. Very similar biases are observed when CMOD4 winds are compared to collocated ECMWF first-guess winds (FGAT; first-guess at proper time). This comparison is part of the monitoring of ERS's wind and wave products that is routinely performed at ECMWF. The wind speed biases have been present since the start of the monitoring in February 1996. Recent experimental work (Donnely *et al.* 1999, Carswell *et al.* 1999) confirm the high wind speed trend. They showed

that beyond 20 $\mathrm{m\,s^{-1}}$, the level of backscatter becomes less sensitive to the wind. In fact, for small incidence angles an over-saturation was observed, i.e., for winds larger than 25 $\mathrm{m\,s^{-1}}$, backscatter starts to decrease. The work of Donnely *et al.* (1999) and Carswell *et al.* (1999) also indicates that for strong winds both the upwind-downwind asymmetry and the upwind-crosswind term are over-estimated by CMOD4. This over-estimation can also be deduced from an internal consistency check. The distance to cone appears to rise rapidly towards higher wind speeds, which indicates that the diameter of the CMOD4 cone is inadequate. Although the upwind-downwind and upwind-crosswind terms will not influence the performance of retrieved wind speed too much, they will have an effect on the quality of ambiguity removal, resp. the accuracy of the wind direction.

The non-optimal behavior of CMOD4 wind biases was reason to update this model function. This work was performed at the Royal Netherlands Meteorological Institute (KNMI) by de Haan and Stoffelen (2001). Its starting point was CMOD4. Wind-speed biases were resolved by relabeling wind speeds before they were presented to CMOD4. Corrections for the upwind-downwind term were applied as well by multiplying the corresponding term in CMOD4 by an attenuation factor that depends on wind speed and incidence angle. No corrections for the upwind-crosswind term were included. The result, from now on denoted by CMOD5(KNMI), indeed improved the wind-bias levels for all wind sectors. In particular, for extreme wind situations, more realistic wind speeds were obtained. Although, averaged over all data, biases were reduced, it appeared that there was still a residual incidence-angle dependent bias. Besides, CMOD5(KNMI) mainly relabels CMOD4; it hardly changes the cone structure. Therefore, this approach does not allow for any misfits between the data-triplet cloud and the GMF cone. For instance, CMOD4's inappropriate formulation for the upwind-crosswind term is inherited by CMOD5(KNMI). Although CMOD5(KNMI) represents an improvement with respect to CMOD4, there is still a number of issues to be resolved.

The work presented in this paper describes the completion of CMOD5(KNMI). The resulting model function, called CMOD5, was tuned by comparing ERS-2 scatterometer triplet backscatter measurements with collocated ECMWF FGAT winds. The period between 1 August and 31 December 1998 was considered, for which the ERS-2 satellite was operating in a stable nominal mode. It embraced more than 22,000,000 collocations. For the extreme wind sector (winds larger than 25 $\mathrm{m\,s^{-1}}$) statistics are sparse, even for a five-months period. In addition, such extreme situations mainly occur for tropical cyclones, for which FGAT winds are known to be on the low side. For this sector, the experimental work of Donnely *et al.* (1999) and Carswell *et al.* (1999) was used as a guideline. An important ingredient for the determination of CMOD5 was internal consistency. It was demanded that the CMOD5 cone gives a proper representation of the data cone.

In section 2, some details and history on the ERS scatterometers is described. Some general aspects of GMF's are summarized in section 3. The performance of CMOD4 and CMOD5(KNMI) with respect to FGAT winds is presented in Section 4. Section 5 gives a description of the methods that were used to deduce the final form of CMOD5. The remainder of the paper gives a presentation of the performance of CMOD5 w.r.t. CMOD4 and CMOD5(KNMI). In section 6 some general aspects will be addressed. The impact of CMOD5 for extreme-weather situations will be studied in Section 7. Some examples of tropical cyclones will be presented. In Section 8, the performance of CMOD5 will be investigated for several independent periods. It allows for the assessment of the importance of trends in the ECMWF FGAT winds on which CMOD5 is based. In Section 9 some concluding remarks are formulated. The paper ends with an appendix, giving a concise description of CMOD5.

2 The ERS scatterometers

The scatterometers onboard the ERS-1 and ERS-2 satellites (Francis *et al.* 1991) are of identical design. They consist of an active microwave instrument (AMI) emitting RF pulses at C-band frequency (5.3 GHz). Backscat-

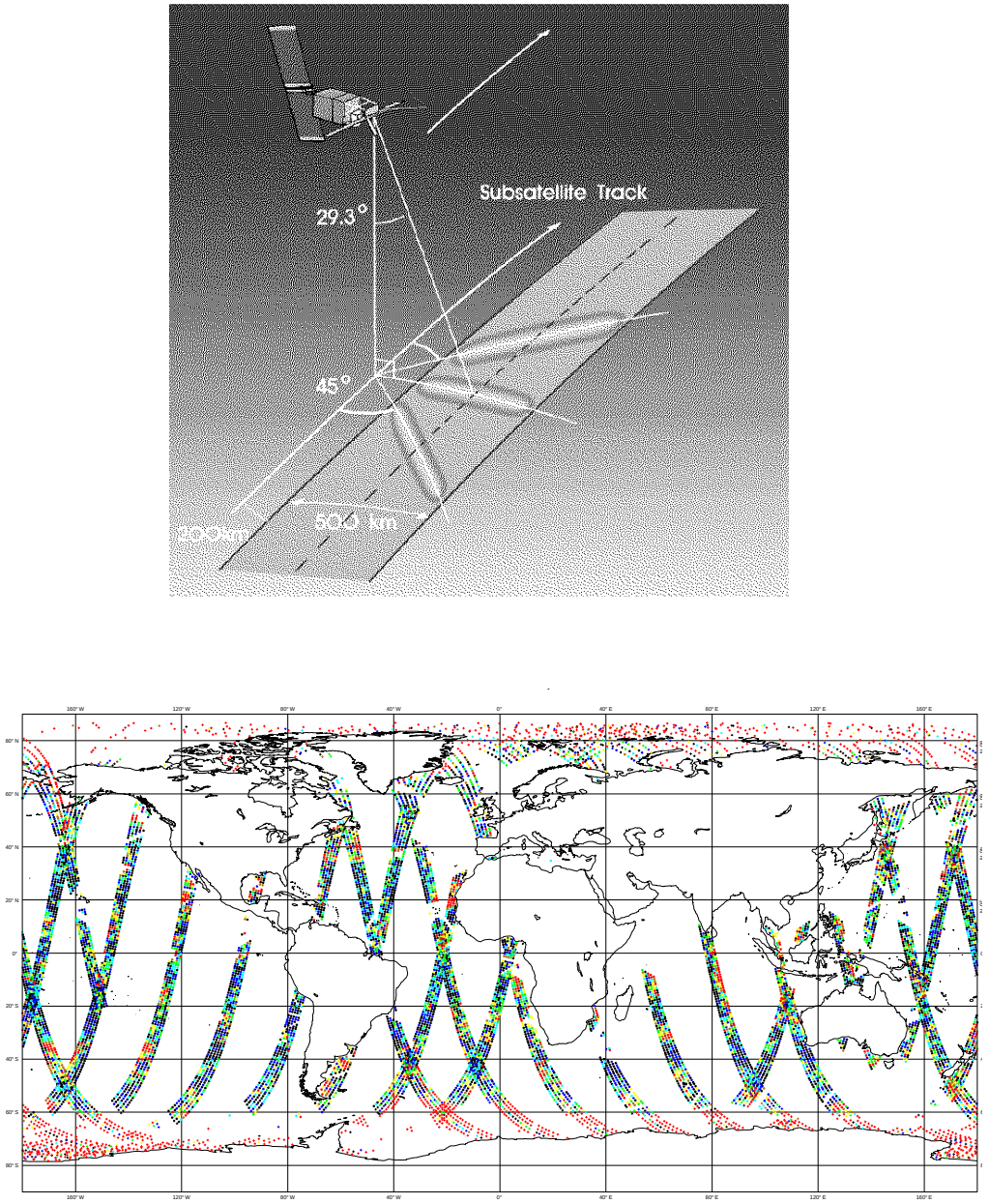

Figure 1: Radar geometry for the ERS scatterometer (top panel) and a typical 12-hour coverage (lower panel).

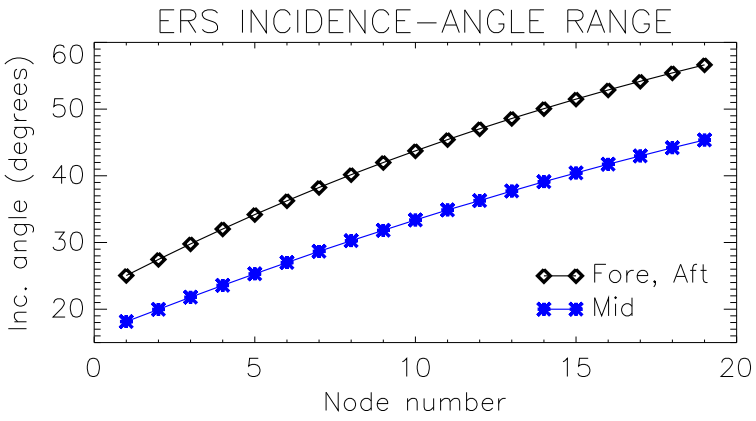

Figure 2: Incidence angle as function of node number for the fore and aft beam (diamond) and mid beam (asterix)

ter measurements are obtained from three antennas: a fore, mid and aft beam pointing to the right side of the spacecraft flight direction at angles of 45^o, 90^o, and 135^o, respectively. They illuminate an area with a swath width of 500 km (see Attema 1986 for details). The ERS satellites are positioned in polar orbits at a height of 785 km; each orbit taking 100 minutes. Within that time, at the equator, the earth has rotated 2,800 km. This means that at low latitudes total coverage of the scatterometers is achieved within a period of three days. At higher latitudes this period is shorter. Due to the inclination of 98.5^o of the orbit, no observations are obtained for latitudes above 80N and below 80S. The configuration of the ERS scatterometers and a typical 12-hourly coverage is displayed in Figure 1.

Inside the 450 km wide swath, 19 nodes define a 25km product. For each such node, average backscatter values are determined from a 50 by 50 km grid, i.e., the 25km product is over-sampled. The incidence angle of the radar pulse on the sea surface depends on node number (see upper panel of Figure 1, and Figure 2). For the fore and aft beam, incidence angles range from 25^o to 57^o, for the mid beam values are somewhat lower (18^o to 45^o).

ERS-1 was launched on 17 July 1991. After its commissioning phase, it has provided scatterometer data from December 1991 until December 1999. In April 1995 ERS-2 was launched. It operated in nominal mode between March 1996 and December 2000. Due to the loss of its gyroscopes in January 2001, a problem in the yaw attitude control arose, which especially affected the quality of scatterometer winds. Since then, the dissemination of ERS-2 scatterometer winds has been suspended. However re-introduction of the data dissemination is expected to take place in January 2003.

3 General aspects of Geophysical Model Functions and wind inversion

3.1 Geophysical model functions

As described in the introduction, backscatter σ_0 depends on wind speed v, the relative angle between the instrument azimuth angle α and wind direction χ, and incidence angle θ. Besides the wind vector, there may also be other geophysical parameters that influence the backscatter. Examples are wave age (incorporated by VIERS), stability of the boundary layer, precipitation (Ku-band only), the presence of slick and confused sea-states. These effects are not taken into account by the CMOD formulations, neither will it by CMOD5. The

main two components for the wind direction dependency are the upwind-downwind and upwind-crosswind effects. Usually higher order effects are neglected. As a result, the general form of the CMOD functions can be written as:

$$\sigma_0^m(v,\phi,\theta) = B0(v,\theta)(1+B1(v,\theta)\cos(\phi)+B2(v,\theta)\cos(2\phi))^{0.625}, \quad (1)$$

where $\phi = \chi - \alpha$. B0 describes the main dependency on wind speed and incidence angle. The Fourier terms $B1$ and $B2$ incorporate the upwind-downwind respectively upwind-crosswind effects. The power 0.625 was introduced in CMOD4 (Stoffelen and Anderson 1997a, 1997b). It was not present in earlier CMOD formulations. Reason for its inclusion was the observation that in σ_0-space cross sections do not look circular. This indicates that higher Fourier terms should be taken into account. However, they found that cone sections did become circular when plotted in a transformed space

$$z = \sigma_0^{1.6}. \quad (2)$$

So for this quantity the omission of Fourier terms higher than order two is a good assumption. Effectively this transformation generates higher order Fourier terms in σ_0-space. In this study results will mainly be presented in z-space.

3.2 Wind inversion algorithms

A GMF predicts modeled backscatter measurements given a local wind field. In practice, a set of backscatter values is observed, from which the best estimate of the surface wind vector is to be estimated. This is achieved by minimizing a cost function in z-space (see Eq.2)

$$\mathrm{MLE}(v,\chi) = \sum_{i=1}^{N}\left(\frac{z^m(v,\chi-\alpha_i,\theta_i)-z_i^o}{k_p[\sum_{i=1}^N z_i^{o2}]^{1/2}}\right)^2. \quad (3)$$

For ERS, N=3, z_i^o is the observed transformed backscatter of the i-th beam (fore, mid, aft) and α_i, θ_i is its azimuth resp. incidence angle. The normalization factor k_p gives an estimate for the relative accuracy of the observation. It is based on a formulation given by Stoffelen and Anderson (1997a):

$$k_p^2 = \frac{1.25}{100} * (1+\frac{45-\theta_2}{27})(1+\frac{5}{v})(1+\frac{1}{v^2})\sqrt{1+0.01\max(v-15,0)^2}. \quad (4)$$

At ESA, the optimization of Eq.(3) is based on the PRESCAT algorithm. This code makes use of a pre-calculated look-up table (LUT) in σ_0-space of the GMF as function of wind speed (from 1 to 60 $\mathrm{m\,s^{-1}}$ in 0.5 $\mathrm{m\,s^{-1}}$ bins), relative wind direction (in 5 degree bins) and incidence angle (from 15 to 69 degrees in 1 degree bins). Backscatter is linearly interpolated to the correct incidence angle. However, no interpolation is applied for wind speed and direction. As a result, the resolution of ESA's wind product is 0.5 $\mathrm{m\,s^{-1}}$ in speed and 5 degrees in direction (i.e., relative to the mid beam azimuth direction).

The PRESCAT algorithm determines for each wind direction (i.e., in 5 degree bins) the wind speed that minimizes Eq.(3). Starting point is a first-guess speed, which for the first direction is based on an analytic inversion in which $B1$ is neglected. For other directions the optimal speed of the previous direction is used as the starting point. The resulting relation between minimal MLE and wind direction is smoothed, after which its local minima are determined. The lowest minimum defines the rank 1 wind solution, the second one (usually nearly anti-parallel) the rank 2 solution. On the basis of collocated short-range ECMWF forecast fields and spatial constraints it is determined which of the two solutions is the preferred one (ambiguity removal, see e.g., Stoffelen and Anderson 1997c).

In 1992 a version of PRESCAT has been implemented at ECMWF as well. For the wind inversions presented in this report, the following two adaptations to the PRESCAT code were performed. Firstly, the LUT was

calculated for z-space, rather than for σ_0-space. Interpolations were performed w.r.t. this quantity. It prevents numerous expensive transformations from σ_0 to z, and has a substantially beneficial effect on computing time. No noticeable differences in resulting winds were observed.

Secondly, due to the over-saturation of CMOD5(KNMI) and CMOD5 backscatter levels, these model functions give rise to two local minima in each wind direction, rather than one; a solution for moderate winds and one for extreme winds. It occasionally happens that for a certain wind direction PRESCAT obtains the extreme wind solution. For the next direction, PRESCAT will start from this point, which makes it difficult to jump to the moderate wind solution, even when that is the better one. As a result, PRESCAT will return an extreme wind solution ($\sim 50 \mathrm{m\,s^{-1}}$), which, when compared to FGAT winds (typically 15 to 20 $\mathrm{m\,s^{-1}}$), is the wrong solution. This inadequacy appeared to occur only for the lower nodes, since for those incidence angles the over-saturation in the model function is strongest (Donnely *et al.* 1999, Carswell *et al.* 1999). To avoid this complication, the first-guess speed in each direction was limited to 20 $\mathrm{m\,s^{-1}}$ (Stoffelen, personal communication 2002). Whenever for a certain direction a higher wind speed is obtained, the minimization in the next direction will start with 20 $\mathrm{m\,s^{-1}}$. This adaptation appeared to work well for all winds regarded in the 5-months period (i.e., over 22,000,000 cases). All cases for which originally the extreme solution was incorrectly obtained, now gave rise to the moderate solution. In addition, these moderate solutions matched well with the collocated FGAT winds.

For CMOD4 the adapted version of PRESCAT gave almost identical results (not shown) to the ESA wind product. The main difference is that the last digit of the newly inverted winds were 0 and 5, while for the ESA winds this is 0, 6 respectively. Another difference is that only one ESA wind solution is available (the de-aliased one). For inverted winds (CMOD4, CMOD5(KNMI), CMOD5) in the present study, both solutions are available. De-aliasing of these winds was based on a collocation with FGAT winds.

4 A comparison between CMOD4, CMOD5(KNMI) and ECMWF first-guess winds

As mentioned in the introduction, observed bias levels of CMOD4 winds are also observed when compared to FGAT winds. In Figure 3 scatter plots between these winds are displayed for the entire optimization period. For plotting reasons, the in 0.5 $\mathrm{m\,s^{-1}}$ resolution available CMOD4 winds were randomly perturbed using a uniform distribution from -0.25$\mathrm{m\,s^{-1}}$ to +0.25$\mathrm{m\,s^{-1}}$. It does not affect bias levels and its impact on standard deviations is in the order of 0.01$\mathrm{m\,s^{-1}}$. The top left panel of Figure 3 presents the average over all nodes. It clearly shows the sinusoidal bias behavior for medium wind-speeds as they were observed by Stoffelen (1998). Also the under-determination of strong winds is evident. Besides, there is an overall negative bias of nearly 0.5 $\mathrm{m\,s^{-1}}$. This bias appears to be node-dependent as can be seen from the other panels of Figure 3. The bias is worst for the first node (almost -1 $\mathrm{m\,s^{-1}}$, top right panel), becomes less towards higher nodes and is more or a less stable ($\sim 0.4 \mathrm{m\,s^{-1}}$) between nodes 10 (lower left panel) and 19 (lower right panel). The standard deviation between the CMOD4 winds and FGAT winds are between 1.54 $\mathrm{m\,s^{-1}}$ for node 5 and 1.61 $\mathrm{m\,s^{-1}}$ for node 19. The average is 1.59 $\mathrm{m\,s^{-1}}$. For nodes 18 and 19, there is a cloud of points with low FGAT winds and too high CMOD4 winds. This cloud is less or not visible for the other nodes. This mismatch will be addressed in more detail in Section 5.1.3.

Scatter plots for the same period, but now based on CMOD5(KNMI) winds, are displayed in Figure 4. The wind-speed dependent bias has largely been removed (top left panel). Also, for strong winds, the agreement with FGAT winds is much better. The overall bias is much smaller (-0.17$\mathrm{m\,s^{-1}}$). However, like for the CMOD4 winds there is still a node-dependent bias. For node 19 the cloud for small FGAT winds and high inverted winds is also present for CMOD5(KNMI).

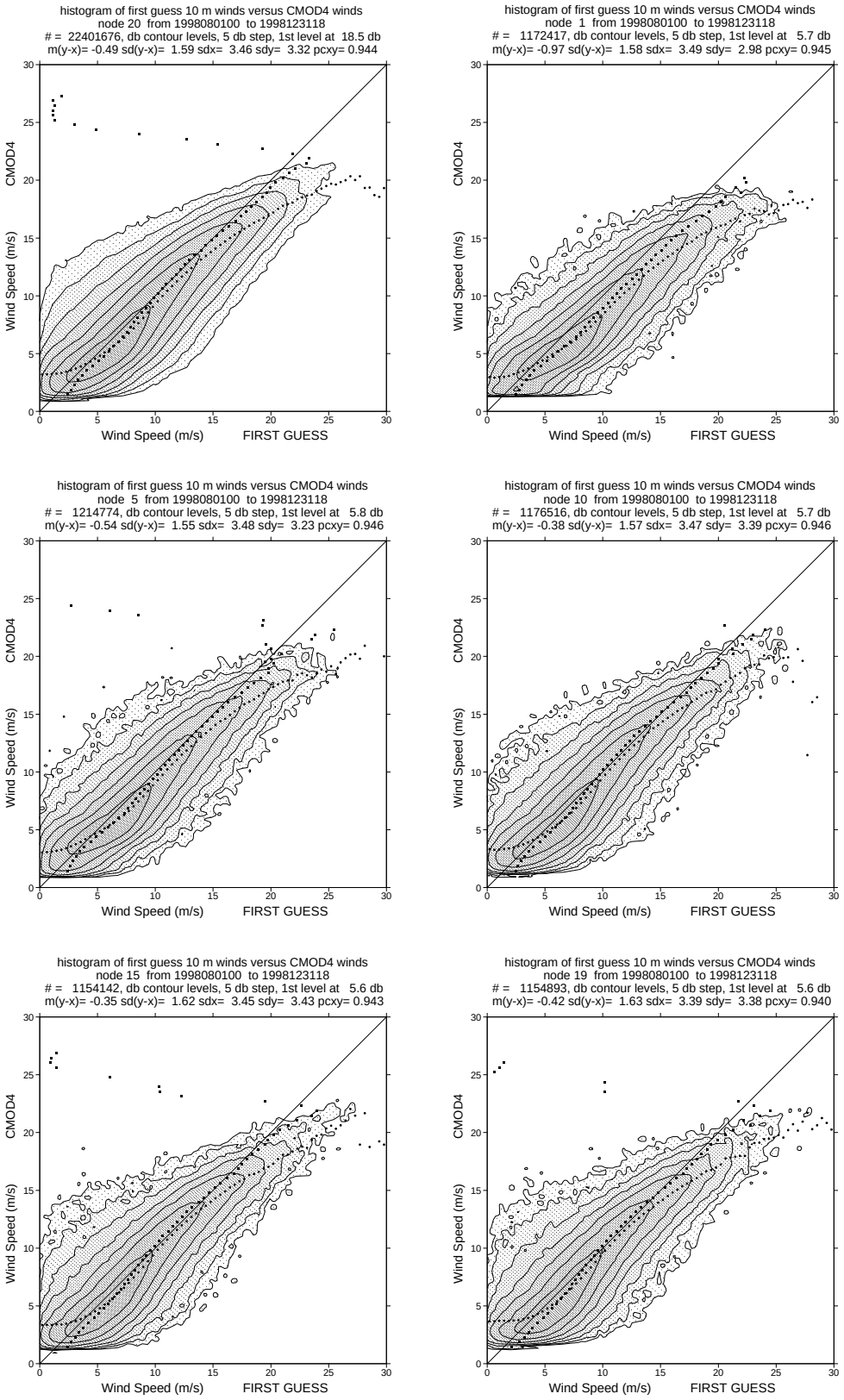

Figure 3: Scatter plot between de-aliased CMOD4 winds and ECMWF FGAT winds for all nodes, and nodes 1, 5, 10, 15 and 19.

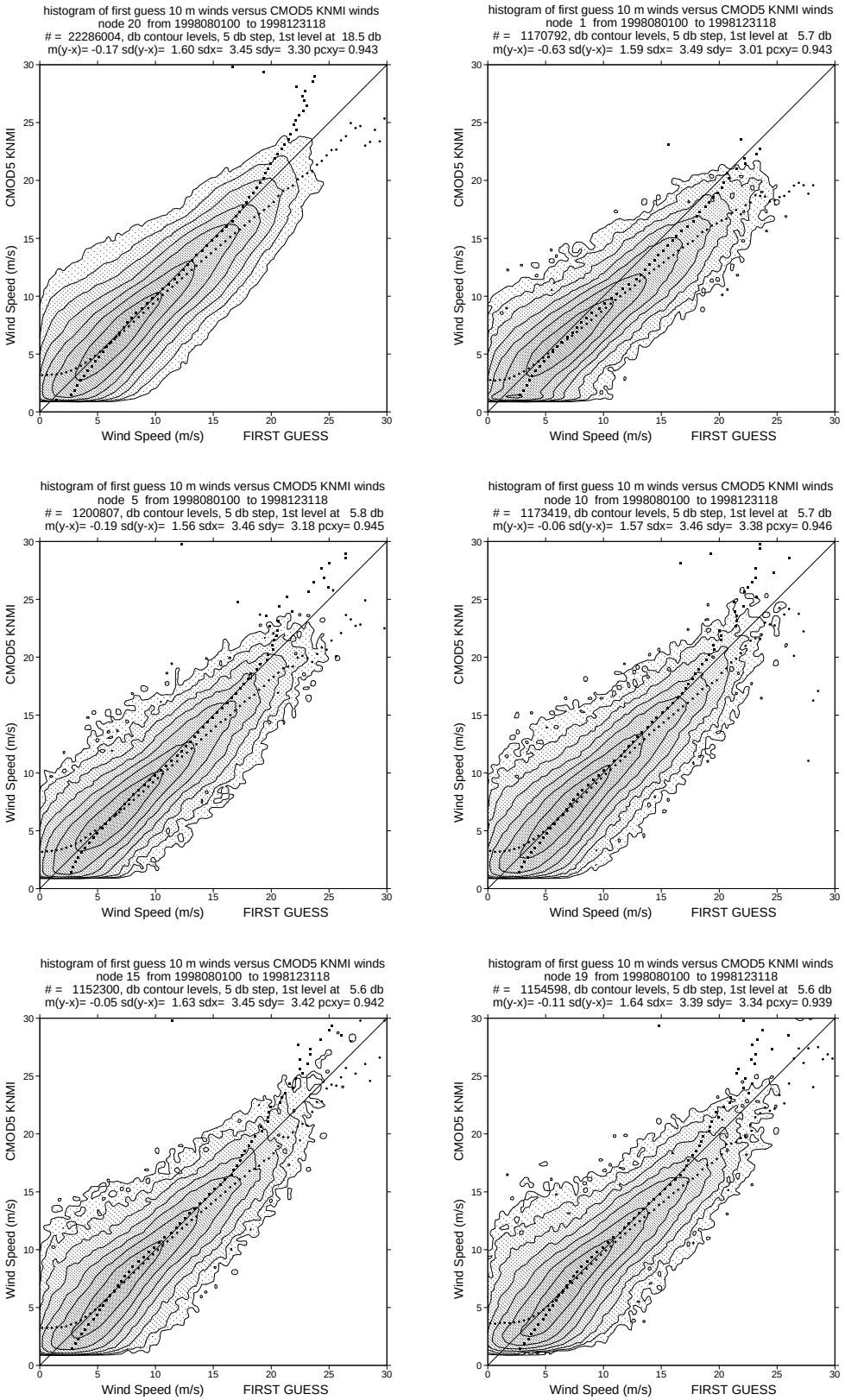

Figure 4: Scatter plot between de-aliased CMOD5(KNMI) winds and ECMWF FGAT winds for all nodes, and nodes 1, 5, 10, 15 and 19.

As was mentioned in the introduction, $B1$ was only updated for high winds and $B2$ was not modified at all. Therefore, CMOD5(KNMI) will not change the cone structure; it mainly relabels wind speed. This is confirmed by Figure 5, which shows a scatter plot between de-aliased CMOD5(KNMI) and CMOD4 winds. The scatter in both wind speed and direction is very small and is mainly induced by the discretization of the wind products. The sinusoidal shape for the wind speed represents the bias correction for low and medium winds; the sharp increase for strong winds the enhancement of CMOD5 winds in this region.

Some examples of the cone structure are shown in Figure 6. Plotted are backscatter triplets for which the sum of z_{fore} and z_{mid} are within a small range. If one neglects the $B1$ term, and bears in mind the geometry of the scatterometer, it is easily derived that by approximation:

$$z_0 \equiv \frac{z_{\text{fore}}+z_{\text{aft}}}{\sqrt{2}} \approx B0^{1.6}(v,\theta_f), \tag{5}$$

$$z_1 \equiv \frac{z_{\text{fore}}-z_{\text{aft}}}{\sqrt{2}} \approx \left[B0^{1.6}(v,\theta_f)B2(v,\theta_f)\right]\,\sin(2\phi_2), \tag{6}$$

$$z_m \approx B0^{1.6}(v,\theta_m) + \left[B0^{1.6}(v,\theta_m)B2(v,\theta_m)\right]\,cos(2\phi_2). \tag{7}$$

Here, ϕ_2 is the wind direction relative to the azimuth angle of the mid beam. So for a given node, stratification of the data w.r.t. z_0 is more or a less equal to stratification to wind speed. In a plane of constant z_0, the data should be distributed around an ellipse defined by Eqs.(6) and (7). Its size is determined by $B2$ of the mid and fore/aft beam. Going from 0 to 360 degrees, the cone winds twice. The non-zero part of $B1$ makes that a constant z_0-plane does not coincide with constant wind speed anymore, and that the second winding is shifted w.r.t. the first one (see e.g., Stoffelen and Anderson 1997a, 1997b). The color coding of the backscatter triplets is determined by the collocated FGAT wind direction, relative to α_2. Purple points are for directions between 0 and 180 degrees, green for directions between 180 and 360. For some cuts the asymmetry introduced by $B1$ can clearly be seen (e.g., z_0=0.08 for node 19). Cuts of the CMOD4 (blue) and CMOD5(KNMI) (black) cone are displayed in Figure 6 as well. Indeed, they nearly overlap. Only for high wind speeds there is a small difference, which is induced by their difference in $B1$. For moderate wind speeds (top panels, see caption for the explanation of wind-speed ranges), the agreement between the data cloud and CMOD cones is reasonably good. For the first node (left panel), $B2$ looks fine, however for nodes 10 and 19 it might be a bit too small. For node 1 the position of the cone looks somewhat too high, which indicates a small inadequacy in the $B0$ term for the mid beam (see Eq.(7)). For strong winds (lower panels) the agreement between the CMOD cones and data cloud is much worse. For node 10 and 19 the CMOD cones are clearly too large. This is exactly what was observed by Donnely *et al.* (1999) and Carswell *et al.* (1999). For node 1, $B2$ looks correct for the fore-aft beam, however, it is too small for the mid beam. Besides, the large shift in the vertical indicates a systematic misfit for the mid-beam $B0$ at that incidence angle. From the lower panels of Figure 6 it may also be deduced that for the middle to higher nodes, $B1$ is too large for strong winds.

5 Determination of CMOD5

5.1 Methods and tools

In this section the methods used to determine the CMOD5 formulation and the tools to check its properties during the development stage are presented. Results are based on data for the five-months period between September and December 1998, and winds were inverted on the basis of the modified PRESCAT code as described in Section 3.2.

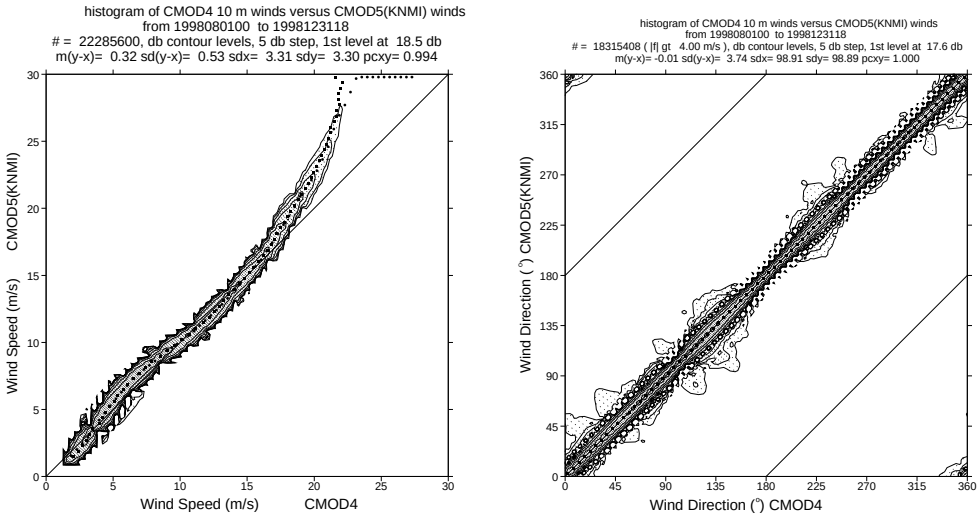

Figure 5: Scatter plot between de-aliased CMOD4 winds and de-aliased CMOD5(KNMI) winds for wind speed (left panel) and wind direction (right panel).

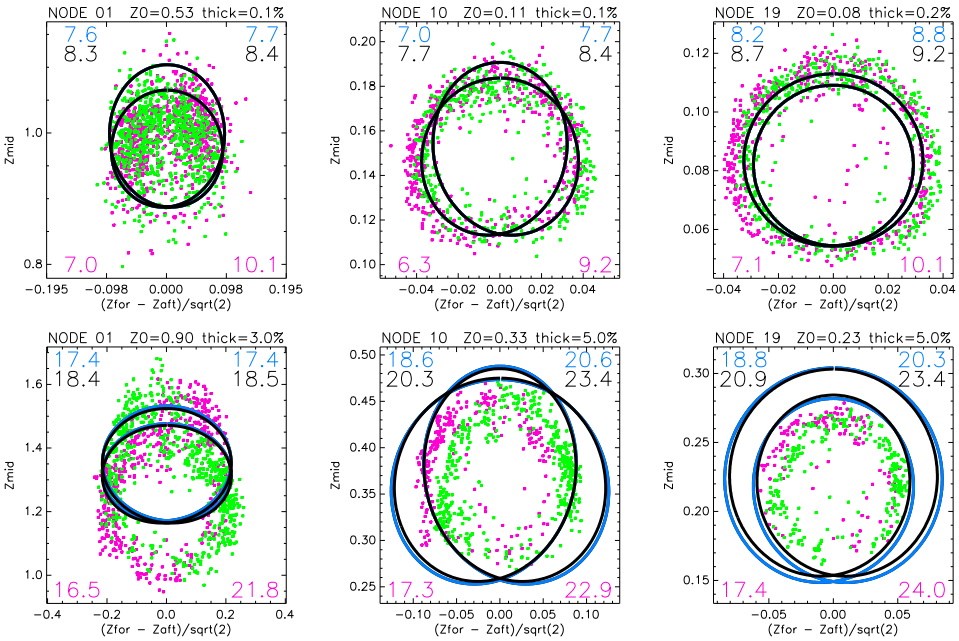

Figure 6: Cone slices for nodes 1 (left), 10 (middle) and 19 (right) for different values of $z_0 = (z_{\text{for}} + z_{\text{aft}})/\sqrt{(2)}$ and thickness. Blue curves are cuts of the CMOD4 cone, black curves for CMOD5(KNMI). Purple points are observed triplets for which the relative wind direction w.r.t. the mid-beam azimuth angle of collocated FGAT winds was between 0 and 180 degrees, green points for directions between 180 and 360 degrees. Numbers within the panels indicate average wind speed plus and minus one standard deviation (left, right resp.) for CMOD4 (blue), CMOD5(KNMI) (black) and collocated FGAT winds (purple).

5.1.1 *Fourier analysis*

For each beam, the dependency on wind direction is modeled according to a sum of a few Fourier terms (see Eq.1). If one neglects errors in the collocated FGAT wind speeds and directions, then these terms can be determined in a straightforward way. For this the data is first stratified according to node number, beam, and FGAT wind speed (bins of 1 $\mathrm{m\,s^{-1}}$). For each such constructed subset, the Fourier terms can be estimated by minimizing the following cost function in z-space:

$$J(A_0,.,A_K) = \sum_i w(\chi_i) \left(\sum_{k=0}^{K} \mathrm{A_k} \cos(k\phi_i) - z_i^o \right)^2, \tag{8}$$

where the sum i is over observations in the subset. The terms A_k are related to $B0$, $B1$ and $B2$ by:

$$B0 = A_0^{1.6}, \qquad B1 = A_1/A_0, \qquad B2 = A_2/A_0. \tag{9}$$

The weight function w is introduced to ensure that each wind direction contributes equally. It was determined for each speed bin separately, by making a histogram of the FGAT wind direction for the five-months period. After some directional smoothing, the weight was taken to be inversely proportional to this histogram. Examples for some speed bins are presented in Figure 7. For very light winds (up to 2 $\mathrm{m\,s^{-1}}$, not shown), the distribution is uniform. For winds between 2 and 10 $\mathrm{m\,s^{-1}}$ easterlies dominate (therefore, smaller weight), and towards stronger winds westerlies start to prevail. Due to lack of statistics the distribution for winds between 19-20 $\mathrm{m\,s^{-1}}$ was used for all winds stronger than 20 $\mathrm{m\,s^{-1}}$. Minimization of Eq. (8) requires the inversion of the matrix equation:

$$C\mathbf{A} = \mathbf{Z}, \qquad \text{where} \qquad C_{kl} = \sum_i w_i \cos(k\phi_i)\cos(l\phi_i) \quad \text{and} \quad Z_k = \sum_i w_i \cos(k\phi_i)\, z_i^o, \tag{10}$$

which, for the obvious cut-off $K = 2$, is easily solved by standard numerical methods. For most subsets, matrix C will be almost diagonal by construction of the weight function w, i.e., $C \approx \mathrm{diag}(1, 1/2, ..., 1/2)$. For such cases, inversion (10) reduces to the standard way of determining Fourier components. However, the minimization method is numerically more stable, and is less sensitive to inaccuracies in the weight function.

The Fourier decomposition is determined for each subset independently, i.e., for each speed bin and each beam. It does not require any knowledge on the relationship between beams or observed triplets, and does not require any wind inversions. It is a direct and simple method which yields point-wise estimations of the $B0$, $B1$ and $B2$ terms as function of wind speed and incidence angle (determined by beam and node number, see Figure (2)). Examples for two incidence angles are shown in Figure 8. Top panels concern the node 4 fore and aft beam ($\theta = 32.0$ degrees) and the node 9 mid beam ($\theta = 31.8$ degrees); lower panels the node 11 fore and aft beam ($\theta = 45.4$ degrees) and the node 19 mid beam ($\theta = 45.4$ degrees as well). Differences in incidence angles are small, and, therefore, the curves for the three beams should overlap within their statistical accuracy. To a large extent this is indeed observed. Especially the overlap for winds between 5 and 25 $\mathrm{m\,s^{-1}}$ for $B0$ gives confidence on the equality of the three beams in this speed range. However, for winds below 5$\mathrm{m\,s^{-1}}$ it is seen that the mid beam for node 19 behaves differently from the fore and aft beam for comparable incidence angle. The asymmetry is connected to the data cloud for high CMOD winds and low FGAT winds in Figures 3 and 4. It is also observed for lower incidence angles, though less profound (not shown). The inter-beam agreement looks somewhat less for $B1$ and $B2$. However, the statistical accuracy is lower as well, since these terms are based on differences between observations (induced by $\cos(k\phi)$). Bearing this in mind, the beams do agree quite well.

The weakness of the Fourier method is that it does not account for errors in the collocated FGAT winds. These winds are believed to have a Gaussian error structure in their u and v-components. Although the exact value of

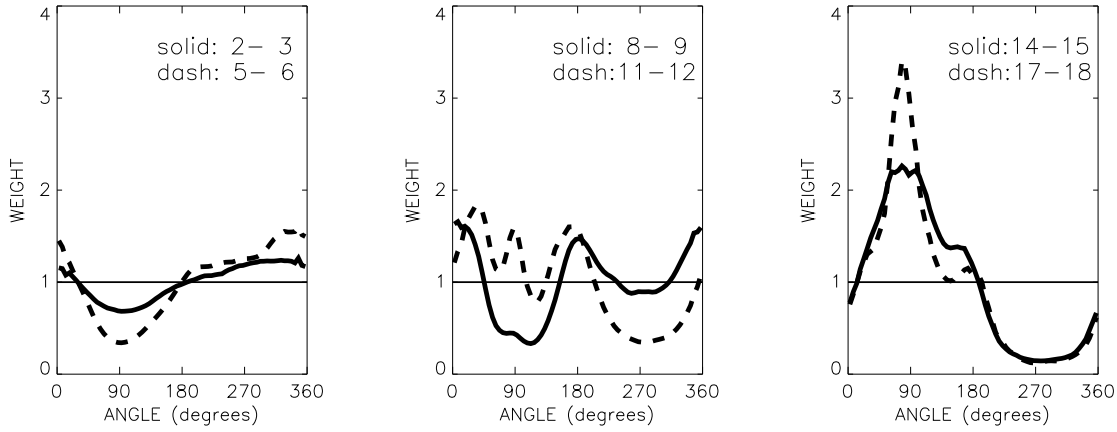

Figure 7: Wind-direction weight distributions based on FGAT winds between August and December 1998, stratified into speed bins of 1 ms^{-1}. Directions are in meteorological convention (0: northerlies, 90: easterlies, 180: southerlies and 270 degrees: westerlies).

its standard deviation is not known, it is believed to be in the range of 1 $\mathrm{m\,s^{-1}}$. For moderate winds this gives rise to accurate wind directions. However, for small winds, large directional errors are to be expected. Such errors have a blurring effect on the Fourier decomposition, especially on the higher order terms, which require more accuracy in wind direction. As can be seen in the right panels of Figure 8, $B2$ goes to zero towards small winds, which is purely an effect of the loss in skill in wind direction of the FGAT winds.

Errors in wind direction should not influence the determination of $B0$. However, for this term, it is the error in the FGAT wind speed that will introduce erroneous results. Within each subset, the binned FGAT winds result from a range of true wind speeds. It are these true speeds that determine the level of backscatter. It can be shown (see e.g. Stoffelen 1998) that FGAT winds result from true winds that are on average somewhat stronger. It is induced by the fact that the distribution of true winds as function of wind speed linearly goes to zero:

$$\rho(v)dv = \int_{v\leq|\mathbf{v}|\leq v+dv} \rho(\mathbf{v})d\mathbf{v} \approx 2\pi\rho(\mathbf{0})\,v \qquad \text{for small } v. \tag{11}$$

Therefore, light FGAT winds are more likely to originate from stronger true winds than from lighter ones. The assumption that the error structure of FGAT winds is Gaussian in its components rather than in speed and direction, enhances this effect even more. For light FGAT winds, the shift in the average true wind speed is in the order of the FGAT wind-speed error. In addition, due to the nonlinear relation between wind speed and backscatter, the backscatter values of the stronger true winds will dominate the average backscatter level within a FGAT wind-speed bin. Both the wind-speed shift and the nonlinearity between wind and backscatter, contribute to the observation that $B0$, as determined by the Fourier method, saturates for light winds. It does not reflect the proper behavior of $B0$.

For the determination of $B1$, the situation is more positive. Firstly, its weak dependency on wind speed makes that errors in this quantity do not contribute substantially. Secondly, $B1$ is also rather insensitive to errors in wind direction, because it effectively tests the difference in backscatter between anti-parallel FGAT winds. This allows for some inaccuracy in wind direction. Although $B1$ vanishes for zero wind speed as well, the situation is much less dramatic than for $B2$.

Abovementioned limitations on the Fourier method were confirmed by experiments in which FGAT winds were taken as true winds. Observations were created from these winds by application of CMOD5(KNMI) plus 5% noise. FGAT winds were created by adding Gaussian noise to the components of the true wind. Several noise

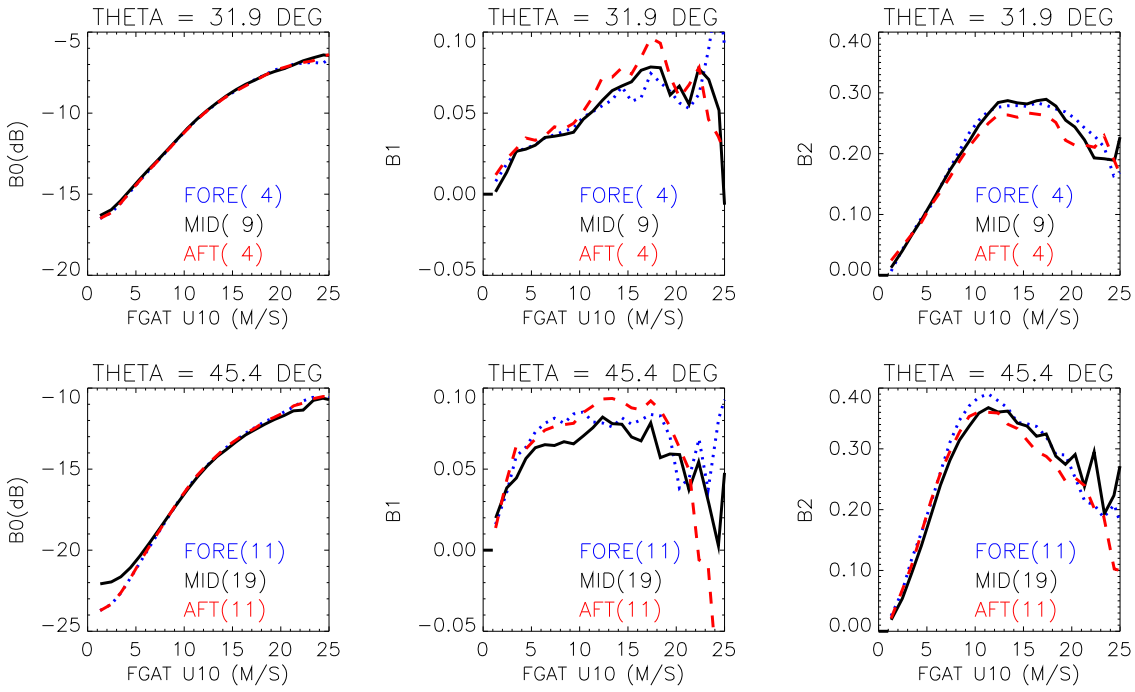

Figure 8: Determination of B0, B1 and B2 on the basis on a Fourier decomposition for subsets of data stratified w.r.t. node number, beam and FGAT wind speed. For each plot, the difference in incidence angles between the fore (dotted), mid (solid) and aft (dash) beam is less than 0.2 degrees.

levels, varying between 0.8 $\mathrm{m\,s^{-1}}$ and 1.4 $\mathrm{m\,s^{-1}}$ were tested. All experiments showed, although less significant than for the real data, the saturation of $B0$ and the vanishing of $B1$ and $B2$. It may be concluded that the Fourier method can not be used for $B0$ and $B2$ for light winds (say below $5\mathrm{m\,s^{-1}}$). For $B1$ and for moderate to strong winds in general, this method does provide useful results.

To circumvent the problems induced by errors in the FGAT winds, one could also stratify bins w.r.t. inverted wind speed [1]. In such case, the Fourier method can be seen as a kind of internal consistency check. The following reflections may make this statement plausible. Suppose that the model function under consideration would perfectly fit the data. Then, the Fourier method will simply reconstruct $B0$, $B1$ and $B2$. In reality, of course, the backscatter measurements have errors ($\sim$ 5%) that will lead to errors in inverted wind speed and direction. However, due to the progressive relationship of backscatter as function of wind speed, these errors are expected to be limited and will not significantly shift average values. The main effect will be that the minimum values of the cost functions given in Eq. (10) will become less optimal. If the considered model function is not too far from the optimal one, then minimizing of of Eq. (10) will result into a new cost function that better fits the backscatter triplets in 3D measurement space, which is, therefore, better. Some iterations should lead to the optimal model function.

Note that this internal consistency check only tests whether the model function cone fits the data well. It doesn't give any information on the relation of the parameterization with the geophysical parameter (wind vector). For instance, a wind speed transformation will leave the cone structure unaltered, as it is the case for CMOD5(KNMI) versus CMOD4 (see Section 4). Therefore, the Fourier method applied to inverted winds will not give information on $B0$. For this the comparison to independent wind information, such as FGAT fields, is essential. For $B1$ and $B2$ this method will result in better formulations of these terms, although they might be

[1] Courtesy of Ad Stoffelen

parameterized w.r.t. a quantity that is not exactly equal to wind speed. However, variations of these terms as function of wind speed are rather slow. Therefore, as long as this quantity does not differ too much from wind speed, the error introduced by this mismatch will be limited.

Since the two wind solutions are nearly anti-parallel, the determination of $B2$ will hardly depend on which rank is used in the Fourier method. On the other hand, for $B1$ the choice of the correct ambiguity is crucial. A proper determination of $B1$ therefore requires a de-aliasing with regard to, for instance, FGAT winds.

5.1.2 Wind-bias corrections

If one neglects the effect of $B1$ it was shown in Eq.(5) that the wind speed only depends on the sum of the backscatter values of the fore and aft beam, and that the relation is determined by $B0$ at the incidence angle of these two beams. Although the inversion routine does not neglect $B1$, its resulting wind speed will still to a large extent be dictated by the wind-speed dependency of $B0$. This means that an observed wind-speed bias between FGAT winds and inverted winds can be used to make corrections to $B0$ (for $\theta = \theta_{1,3}$), by relabeling the wind speed.

Starting from a scatter plot between two wind-speed quantities v_1 and v_2 (like CMOD winds versus FGAT winds in Figures 3 and 4), biases can be calculated in two different ways. They may either be based on the average of v_2, given a certain value of v_1, or on the average of v_1, given v_2. Both conditional averages, called a_1 resp. a_2 are formally defined by:

$$a_1(v) = \quad < v_2 | v_1 = v > \quad \equiv v + \alpha_1(v) \tag{12}$$
$$a_2(v) = \quad < v_1 | s_2 = v > \quad \equiv v + \alpha_2(v). \tag{13}$$

The functions $\alpha_{1,2}$ represent the deviation from the diagonal. Examples of these conditional averages are presented in the left (CMOD4) and middle (CMOD5(KNMI)) panels of Figure 9. It is seen that a_1 and a_2 are very close to each other for moderate winds. For light and strong winds, i.e., at the edges of the distribution of the true wind speeds, both curves deviate. Towards light winds (as explained in the previous subsection) and also towards strong winds, the number of true winds decreases. Therefore, a light or a strong FGAT wind is more likely to originate from a stronger resp. weaker true wind. The CMOD winds are random perturbations from such true winds, and will therefore, on average, also be stronger for light and weaker for strong FGAT winds. This makes that a_1 is enhanced for light winds and suppressed for strong winds. The same argument applies for a_2. This effect is not induced by the underlying stochastic relation between the true winds and FGAT respectively CMOD winds. If this relation is Gaussian in wind components, however, for light winds, the enhancement of a_1 and a_2 will be stronger, since the in component space unbiased perturbations from the true wind will result in a positively biased wind speed.

If one makes the assumption that both winds have comparable error structures, it is expected that their scatter diagram should be symmetric around the diagonal. Any deviation of the symmetry line from the diagonal would indicate a bias. To be specific, the curves a_1 and a_2 should be symmetric, i.e., $a_1 = a_2$. Let the bias of v_2 w.r.t. v_1 be given by d, and assume that it is small compared to v_2 itself. Then for a new, unbiased quantity v_2' one has:

$$v_2' = v_2 - d(v_2) \qquad \Longrightarrow \qquad v_2 = v_2' + d(v_2') + O(d^2) \tag{14}$$

Assuming that α_1 and α_2 are also small, then w.r.t. v_2' conditional averages become:

$$a_1'(v) = < v_s' | v_1 = v > \approx \quad a_1(s) - d(a_1(v)) \quad \approx a_1(v) - d(v) \tag{15}$$
$$a_2'(v) = < v_1 | v_2' = v > \approx \quad a_2(s + d(v)) \quad \approx a_2(v) + d(v) \tag{16}$$

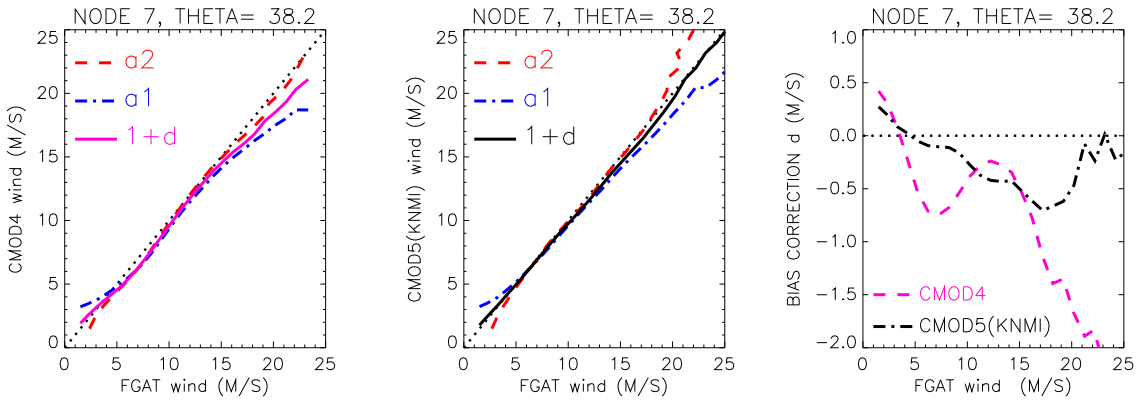

Figure 9: Average conditional wind speeds a_1 and a_2 and bias correction w.r.t. to diagonal $1+d$, for CMOD4 (left panel) and CMOD5(KNMI) (middle panel). Bias corrections d are presented in the right panel.

From the demand that there is no bias between v_1' and v_2 it follows:

$$a_1' = a_2' \qquad \Longrightarrow \qquad d = \frac{1}{2}(a_1 - a_2) \tag{17}$$

So by approximation, the bias between CMOD winds and FGAT winds is given by the half of the difference of their conditional averages. In Figure 9 this bias is plotted w.r.t. the diagonal for CMOD4 (left panel) and CMOD5(KNMI) (middle panel). These curves are situated in between the curves for the conditional averages. In the right panel of Figure 9 the biases themselves are plotted. For this node, the negative bias for CMOD4 increases with wind speed. The bias for CMOD5(KNMI) is smaller, and around -0.5 $\mathrm{m\,s^{-1}}$ between 5 and 20 $\mathrm{m\,s^{-1}}$. Bias levels for nodes 1, 5, 10, 15 and 19 are visible in Figures 3 and 4.

The underlying assumption of the wind-bias correction method is that the CMOD winds and FGAT winds have similar statistical properties. The validity of this assumption is not exactly known. The only thing that can be stated (from scatterplots such as given in Figure 4) is that the sum of their variances is between 1.55 and 1.60 $\mathrm{m\,s^{-1}}$. Estimates of their individual values could be obtained by a triple collocation study with e.g., buoy wind observations (Stoffelen 1998) or QuikSCAT winds. The impact of an unequal error distribution on the correctness of Eq. (17) was tested by taking the FGAT winds as true winds, and creating CMOD winds and new FGAT winds by adding Gaussian noise to the components of the true winds. In case a standard deviation of 1.1 $\mathrm{m\,s^{-1}}$ is applied to both winds, d is zero, as expected. When noise levels of 0.8 $\mathrm{m\,s^{-1}}$ for FGAT winds, and 1.35 $\mathrm{m\,s^{-1}}$ for CMOD winds are applied, d is on average positive (0.1 $\mathrm{m\,s^{-1}}$). When errors are completely attributed to the CMOD winds (1.6 $\mathrm{m\,s^{-1}}$), d is on average 0.2 $\mathrm{m\,s^{-1}}$. These values could be seen as a measure for typical errors introduced by the assumption of equal standard deviations. It is reasonable to believe that neither the FGAT nor the CMOD winds are more accurate than 0.8 $\mathrm{m\,s^{-1}}$. Therefore, typical errors are likely to be in the order of 0.1 $\mathrm{m\,s^{-1}}$.

The assumption that bias levels are relatively small is for some situations not well satisfied. For instance, for small incidence angles, CMOD5(KNMI) has large negative biases (up to -2 $\mathrm{m\,s^{-1}}$) for strong winds. Although relabeling of winds speeds for these cases might not lead to optimal results, it is expected that it will improve the situation. A few iterations of this method should solve the problem.

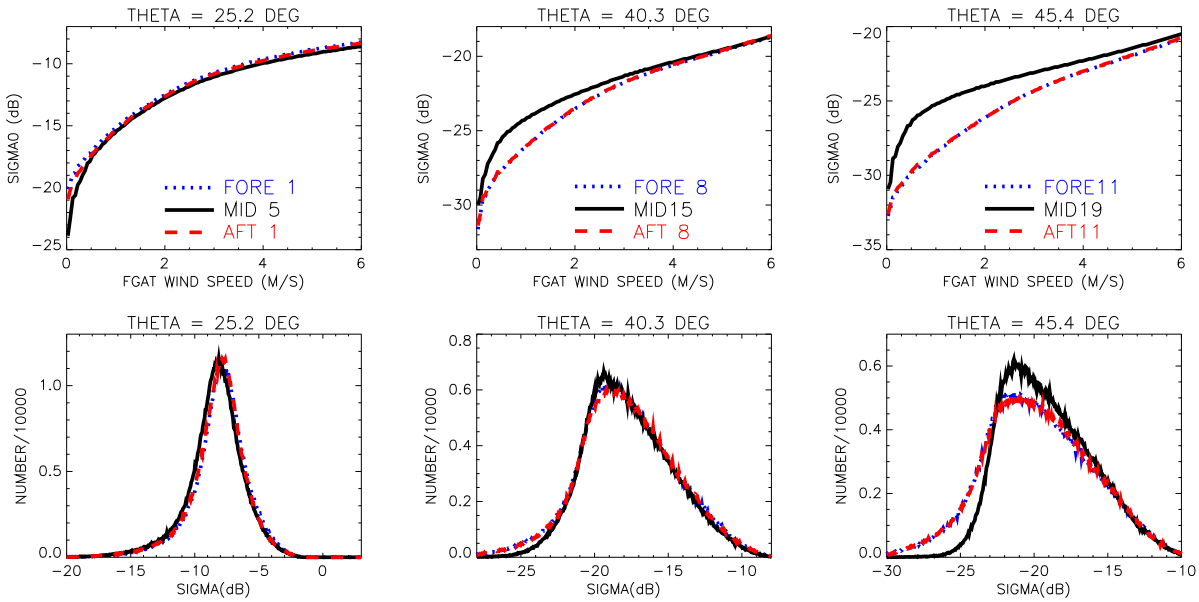

Figure 10: Top panels: relation between wind speed and backscatter, based on statistical grounds. Lower panels: backscatter distribution.

5.1.3 Statistical analysis

The Fourier method described in section 5.1.1 gives too high estimates for $B0$ at low winds. For instance, for node 19, values of -25 dB and -22 dB for the fore/aft resp. mid beam are found, while backscatter values as low as -30 dB are observed. A reason for the too high values (as discussed in Section 5.1.1) is the strong wind-speed dependency of the backscatter in this region, which shifts average values upwards. Small backscatter measurements should be associated with low winds, which gives an indication on the value of $B0$ for such winds. One could make a statistical argument by claiming that the lowest p% backscatter measurements should come from the lowest p% of speed values. Due to the strong speed dependency and weak direction sensitivity at low speeds, two identical backscatter measurements for two different wind directions must stem from nearly identical speeds. Therefore, the error in wind speed introduced by neglecting the $B1$ and $B2$ term is small, which allows for an accurate estimation of $B0$ as function of wind speed. For moderate and strong winds this argument is not valid. But for those regions the Fourier method, respectively the bias-correction method are good alternatives.

In the top panels of Figure 10, estimates for $B0$, based on the statistical argument, are given. Displayed are the cumulative distributions $(U_{10}^{\mathrm{FGAT}}(p), \sigma_0(p))$, $p \in [0,1]$. In order to avoid differences introduced by the difference in azimuth angles for the three beams, the weighting in wind direction as described in section 5.1.1 was applied to these density functions. Although, for small winds the weighting function is nearly uniform, so its omission wouldn't harm results too much.

Like the Fourier method, the statistical method is applied for each beam separately and does not require any inversion of winds. So also for this method, asymmetries between beams can be traced. As expected, lower (more reliable) estimates for $B0$ for weak winds are obtained (top panels of Figure 10). The asymmetry for high incidence angles that emerged for the Fourier method, is also detected here. For the mid beam, estimates of $B0$ are for such angles higher than for the fore and aft beam. Differences start to develop for angles larger than 30 degrees (not displayed) and can be as large as 5 dB for the highest incidence angles (see top right

panel of Figure 10). For lower incidence angles and for winds larger than 5 $\mathrm{m\,s^{-1}}$ in general, the beams behave identically.

The beam-asymmetry can also be observed by looking at the backscatter density functions directly. Examples are displayed in the lower panels of Figure 10 (bin size of 0.05 dB). For low incidence angles the distributions overlap, for high incidence angles backscatter measurements for the mid beam start about 5 dB higher than for the fore and aft beam.

So although the statistical method is well suited to determine $B0$ for low winds, it is the asymmetry between the beams that makes it difficult to decide which curve the model function should be tuned to.

5.1.4 Cone sections

In section 4 it was discussed how to compare the cone defined by a model function with observed triplets by making cuts in planes of constant z_0. Plotting such cuts for different values of z_0 and for all nodes, allows for a visual inspection of the internal position of the model cone in z-space. It is difficult to quantize such an inspection; it is subject to the judgment of the eye.

5.1.5 Extreme winds

Although there were intense tropical cyclones (e.g. Mitch, category 5) and severe extra-tropical storms in the considered five-months period, the amount of such extreme situations will always be limited. Besides, for tropical cyclones, FGAT winds are known to be too low. For the methods used in this paper, statistics were found to be sufficient for winds up to 25 $\mathrm{m\,s^{-1}}$. Beyond this speed, experimental knowledge obtained by Donnely *et al.* (1999) and Carswell *et al.* (1999) is to be used. For the $B0$ term these results were already incorporated in CMOD5(KNMI). Therefore, a convenient way to include the high-wind behavior, is to compare the CMOD5 $B0$ term with the CMOD5(KNMI) $B0$ for winds between 40 and 60 $\mathrm{m\,s^{-1}}$. The saturation behavior, i.e. over-saturation for low incidence angles, and slow saturation for high angles was explicitly modeled by looking at the data of Donnely *et al.* directly. For $B1$ and $B2$ there was no constraint applied other than the way in which both should go to zero for high winds.

5.2 Construction

The CMOD5 model function was constructed using the methods and tools described in the previous subsection. This was achieved in an iterative way. Each term was updated separately, using its own methods. In case these methods required the inversion of winds, i.e., the full knowledge of a model function, the current estimate for the other two terms was used.

The first term that was determined was $B1$, since its construction did not rely on the other two terms. Then $B2$ was determined, using the newly obtained $B1$ and a slightly modified form of the CMOD5(KNMI) definition of $B0$:

$$B0^{\mathrm{start}}(v,\theta) = B0^{\mathrm{CMOD5(KNMI)}}(v',\theta), \qquad v' = v/(1.01+0.067*[1-\tanh(3.2x+1.5)]), \tag{18}$$

where

$$x = \frac{\theta - 40}{25}. \tag{19}$$

This modified $B0$ removes up to first order the residual wind bias for CMOD5(KNMI) at low incidence angles (see Figure 4), while it leaves the behavior at large incidence angles more or less unchanged. Then, $B0$ was

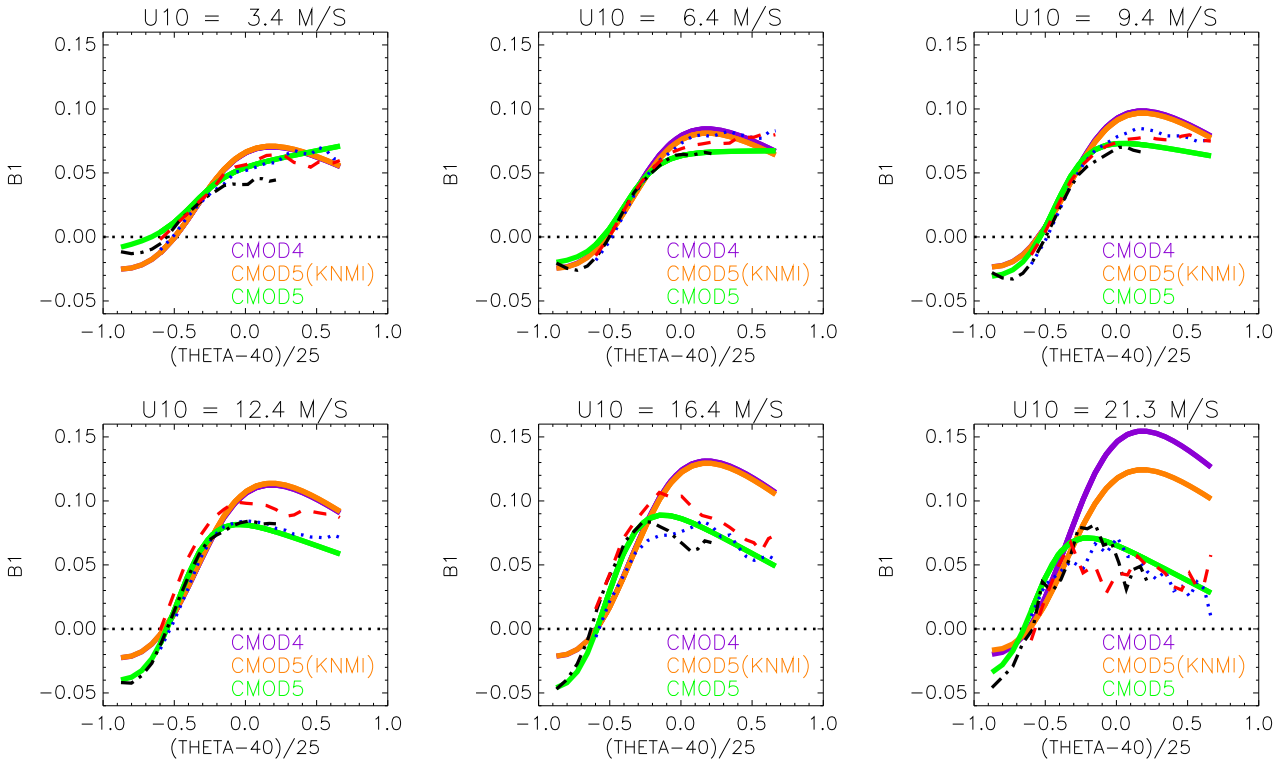

Figure 11: Estimates for the B1 term for the fore (dotted blue), mid (dot-dashed black) and aft (dashed red) beam based on the Fourier method. The corresponding formulations for CMOD4 (purple), CMOD5(KNMI) (beige) and CMOD5 (green) are displayed as well.

optimized, using the new formulations for $B1$ and $B2$. Next, $B2$ was optimized again, using the updated version of $B0$, after which $B0$ was retuned. This procedure was iterated several times, which at the end culminated in the final definition of CMOD5 (see the appendix).

5.2.1 Determination of B1

The term responsible for the upwind-downwind asymmetry was the only term that was determined in a direct way, without using knowledge contained by the other two terms. It was obtained on the basis of the Fourier analysis method described in Section 5.1.1. It does not require the inversion of winds and is determined for each beam and speed bin independently. For six speed bins, the resulting estimates are displayed in Figure 11. No large inter-beam differences were found. Only for winds between 11 and 16 $\mathrm{m\,s^{-1}}$ at incidence angles larger than 30 degrees, the $B1$ term of the aft beam is somewhat larger than for the mid and fore beam. Other differences are not really statistically significant.

The estimate for $B1$ is obtained in a discretized form. Next step was the choice of a functional form that matches these results as good as possible, and in addition, incorporates the experimental results of Donnely *et al.* (1999) and Carswell *et al.* (1999) that $B1$ should approach zero for large wind speeds. The formulation given in Eq. (28) was found to be appropriate. The form of the numerator is similar to the definition of $B1$ for CMOD4. The $\tanh(x) - x$ dependency describes the growth at small incidence angles, and its over-saturation for higher x. It is confirmed by the estimates for the three beams. The denumerator in Eq. (28) is not present for CMOD4. It was included to describe the proper asymptotic behavior. In total, the here proposed $B1$ contains five

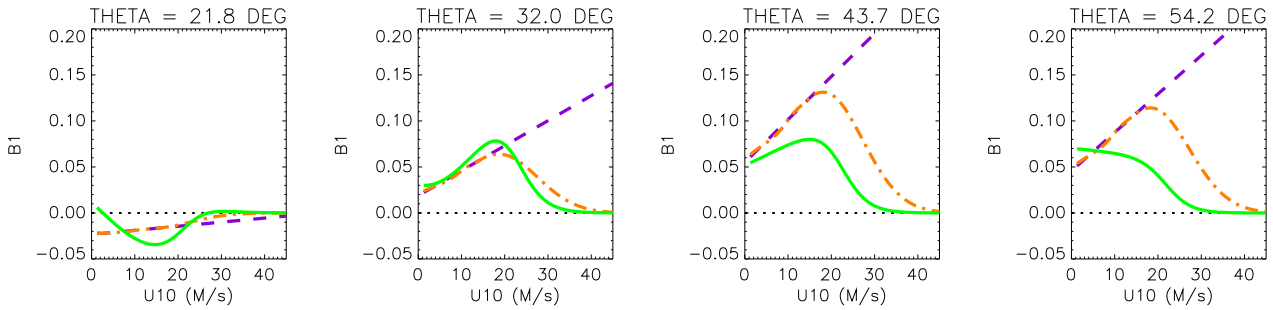

Figure 12: Formulations of the B1 term for CMOD4 (dashed purple), CMOD5(KNMI) (dash-dotted beige) and CMOD5 (solid green).

coefficients, c_{14} to c_{18}. They were determined by minimizing a cost function expressing the difference between the modeled $B1$ and the Fourier estimates of $B1$ for the three beams. The first two speed bins (average winds of 1.3 and 2.4 $\mathrm{m\,s^{-1}}$) were not taken into account, since, due to the limited skill in wind direction of the FGAT winds in this region, the Fourier method gives too low estimates (see Section 5.1.1)). The resulting fit gives a quite good representation of the gridded estimates, as can be seen from Figure 11. Also from this Figure, it is seen that for winds up to 9 $\mathrm{m\,s^{-1}}$ the formulations of CMOD4, CMOD5(KNMI) and CMOD5 are reasonably similar. The same is true for all wind speeds for incidence angles lower than 35 degrees. However, towards high winds, CMOD5 gives much lower values than the other two. This is more clearly seen by plotting $B1$ as function of wind speed. This is for four incidence angles (similar to the ones considered by Donnely *et al.* 1999) displayed in Figure 12. As can be seen, the unrealistic growth towards large winds for CMOD4 is, based on Donelly *et al.* (1999), corrected by CMOD5(KNMI). For this model function, $B1$ does, by construction, go to zero. However, for CMOD5 the onset to this asymptotic behavior occurs quicker, since this emerged from the Fourier analysis.

5.2.2 Determination of B2

As was discussed in Section 5.1.1), the Fourier method is not expected to give reliable estimates for $B2$ for winds lower than 5 $\mathrm{m\,s^{-1}}$. If one, however, has some confidence on the quality of the $B0$ term, it was argued in Section 5.1.1 that stratification w.r.t. inverted winds, rather than FGAT winds, presents a sensible alternative. Results of this method are displayed in Figure 13. Note that these estimates for $B2$ are based on the final CMOD5 model function. However, the first iteration, i.e., $B0$ given by Eq. (18), $B1$ by Eq. (28), and $B2$ by the CMOD5(KNMI) formulation, gave very similar results (which shows that this method has a good convergence). It is clearly seen from this Figure that indeed the estimates for $B2$ go faster to zero for large wind speeds, than the CMOD4 and CMOD5(KNMI) formulations do. Also, it is visible that for winds lower than 5 $\mathrm{m\,s^{-1}}$, $B2$ seems to increase. This effect is strongest at high incidence angles. It is also exactly here where values become higher for the mid beam. This effect is likely associated with the underflow problem and may, therefore, not represent the true behavior of $B2$ in this region.

Like for $B1$, the obtained gridded estimates were to be transformed into functional formulations. As a function of wind speed, $B2$ first grows, has a maximum between 10 and 15 $\mathrm{m\,s^{-1}}$, and then relaxes to zero for large wind speeds. From the extreme-wind behavior obtained by Donnely *et al.* (1999) and Carswell *et al.* (1999) it can be seen that this relaxation is likely to be exponential. The peak for moderate winds can be imposed by multiplying this exponential with a linear function in wind speed. For light winds, the leveling off is to be modeled separately. If this is not done, it was found to be impossible to find proper fits to the estimates based on the Fourier method for all incidence angles and wind speeds. After some trail and error the formulation given

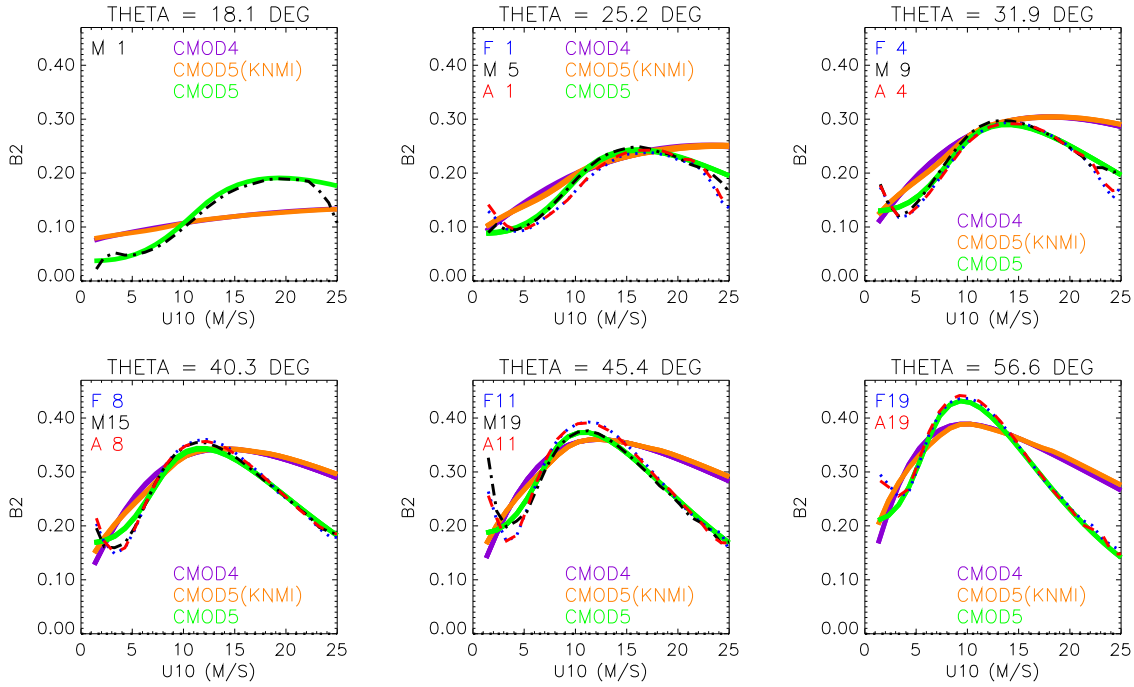

Figure 13: Estimates for the B2 term for the fore (dotted blue), mid (dot-dashed black) and aft (dashed red) beam based on the Fourier method. The corresponding formulations for CMOD4 (purple), CMOD5(KNMI) (beige) and CMOD5 (green) are displayed as well.

by Eqs. (30) to (32). was found to satisfy all requirements. The formulation involves 10 coefficients; eight (c_{21} to c_{28}) determine the detailed incidence angle dependency for moderate to strong winds, while two (c_{19} and c_{20}) model the behavior for light winds. The eight coefficients were determined by minimizing the squared difference between gridded estimates and the modeled form of $B2$ for winds between 9 and 25 $\mathrm{m\,s^{-1}}$. The result was found to satisfy the experimental asymptotic behavior reasonably well. The two coefficients for light winds were subsequently tuned by eye. This involved the performance of cone sections and the performance of the distance to the cone (see next Section).

The resulting curves are presented in Figure (13) as well. As can be seen, the relation to the Fourier estimates is quite close. Besides the improved asymptotic behavior CMOD5 has for several incidence angles somewhat higher peak values than CMOD4 and CMOD5(KNMI). This can also be seen in Figure 14 where $B2$ is plotted

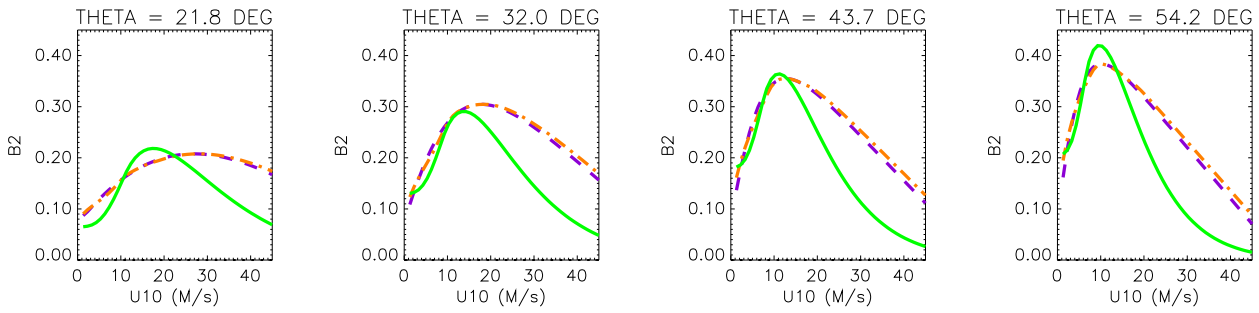

Figure 14: Formulations of the B2 term for CMOD4 (dashed purple), CMOD5(KNMI) (dash-dotted beige) and CMOD5 (solid green).

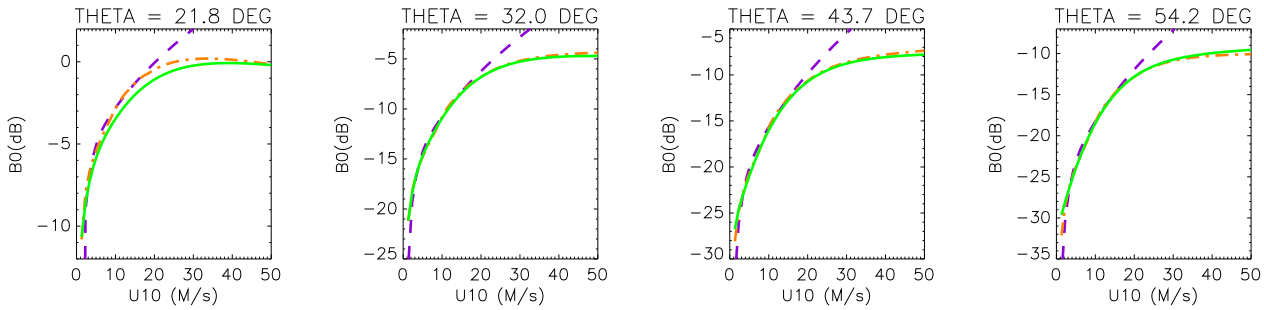

Figure 15: Formulations of the B0 term for CMOD4 (dashed purple), CMOD5(KNMI) (dash-dotted beige) and CMOD5 (solid green).

for incidence angles that were considered by Donnely *et al.* (1999).

5.2.3 Determination of B0

Like for $B1$ and $B2$ the construction of the $B0$ term was performed in two steps. First the scale of $B0$ was determined using the method of wind-bias corrections (section 5.1.2), and then a proper formulation was to be found. Starting point was Eq. (18) for $B0$, Eq. (28) for $B1$ and the first CMOD5 estimate for $B2$. Corrections in $B0$ were introduced by relabeling wind speeds. The magnitude of these redefinitions, or biases (see Eq.(17)), were presented in the form of a table as function of wind speed and incidence angle. Each element was taken to be the central average of three wind-speed bins. Biases were linearly interpolated in both speed and incidence angle. For wind speeds larger than 24 $\mathrm{m\,s^{-1}}$, and for incidence angles smaller than that of the first fore beam (e.g., for the first four mid beam nodes) bias values for 24 $\mathrm{m\,s^{-1}}$, resp. for the first fore beam were used. Given a corrected form for $B0$, and using the current estimates for $B1$ and $B2$, new winds were inverted, leading to new bias corrections and a new estimate for $B0$.

Besides the wind-bias correction method, cone sections were compared with the cloud of backscatter triplets. It was found for the first iterations, that at low incidence angles and high winds, the model cone was shifted upwards w.r.t. the data. This shift is, not surprisingly, also present for CMOD4 and CMOD5(KNMI), as can be seen from the lower left panel of Figure 6. This indicates that $B0$ is too high for the lowest incidence angles. This imperfection can not be detected by the wind-bias method, since that only gives information on incidence angles for fore and aft beams, i.e., not for the first four mid beams. The plotting of cone sections is only a tool to show performance and is not a method that gives direct information on what corrections are to be imposed. Some trail and error was necessary before a description of $B0$ was found for which the cone was correctly positioned.

The resulting description of $B0$ was in the form of Eq. (18) plus a wind relabeling given in a tabular form. From this point a proper functional description was to be designed. In contrast to $B1$ and $B2$, this had to be performed in an extremely careful manner, since differences of 0.2 dB can already lead to differences in wind speed of 0.5 $\mathrm{m\,s^{-1}}$. The total dynamical range of $B0$ is in the order of 30 dB, which may illustrate the required accuracy. The description of $B0$ was split into two parts. A part responsible for moderate and high winds, and a part for light winds. After some research, the form as presented in Eqs. (24) to 27) was found to be appropriate. It depends on 13 coefficients, c_1 to c_{13}.

The saturation behavior for extreme winds is determined by a_1, see Eq.(27). It was chosen to be a linear function of incidence angle, such that there is only over-saturation for angles below 40 degrees. The level of over-saturation was explicitly determined from the data compiled by Donnely *et al.* (1999).

The level of backscatter as function of incidence angle is determined by a_0 (see Eq. (27)). Due to the required accuracy it was found that a third-order dependency in incidence angle was necessary. The quantities a_2 (Eq. (27)) and γ (Eq. (27)) are used to shape the form of b_0. The nine coefficients for these three quantities were optimized by minimizing a cost function, that represented the misfit between the tabulated form of $B0$ and formulation (24). It involved the sum over all incidence angles of the fore/aft and mid beam, and the sum over gridded speed values from 6 to 25 $\mathrm{m\,s^{-1}}$. In addition to this cost, also a term was included representing the misfit between the original CMOD5(KNMI) $B0$ term and formulation (24) for $1\,\mathrm{m\,s^{-1}}$ speed bins between 40 and 60 $\mathrm{m\,s^{-1}}$. In that way, the level of $B0$ for extreme winds was automatically incorporated.

For light winds, $B0$ was chosen to go to zero as a power law, see Eq. (25). The transition between the two wind regimes is continuously differential. Its location is determined by s_0 (see Eq. (27)). This quantity linearly depends on incidence angle. Its two coefficients were determined by comparing the CMOD5 $B0$ formulation with estimates of $B0$ based on the statistical method and by looking at cone sections for low wind speeds.

In Figure 15, the resulting formulation of $B0$ is compared to those of CMOD4 and CMOD5(KNMI) for incidence angles that were regarded by Donnely *et al.* (1999). As is clearly seen, CMOD4 does not saturate, which explains the high negative wind biases for strong winds. For the higher incidence angles, the differences between CMOD5(KNMI) and CMOD5 are small. However, they are larger than 0.2 dB and, therefore, will emerge as noticeable differences in inverted wind speeds. The difference for small incidence angles is larger. It was induced by two imperfections of CMOD5(KNMI) at low nodes: the negative wind bias and the misplacement of the model cone.

The residual wind biases of the final CMOD5 formulation are displayed in Figure 16. It is based on Eq. (17) that was used to update $B0$. Also shown are the biases for CMOD4 and CMOD5(KNMI). From this it is seen that CMOD5 is superior to CMOD4. Bias levels are within a 0.3 $\mathrm{m\,s^{-1}}$ range for all winds below 23 $\mathrm{m\,s^{-1}}$ at all incidence angles. It does not exhibit the bias behavior of CMOD5(KNMI) for the lower incidence angles. Only for high winds at high incidence angles, the CMOD5 winds are somewhat too low.

The 'quality' of the fit of $B0$ for light winds is reflected by Figures 17 and 18, which represent the agreement of $B0$ with the statistical method and the position of the model cone, respectively. From Figure 17 it is seen that CMOD5 matches the statistical curves best. Besides, $B0$ does not go to -60 dB for winds lower than 1, 2 $\mathrm{m\,s^{-1}}$, like is the case for CMOD4 and CMOD5(KNMI). Given the asymmetry between the mid and fore/aft beam, it was chosen to follow the latter two beams as close as possible, since they determine to a large extent the wind speed. For the cone sections the CMOD5 formulation does not improve the situation at low wind speeds. As can be seen from Figure 18, the shift of the cone w.r.t. the mid-beam direction is for high incidence angles higher for CMOD5 than for the other two model functions. It was found to be difficult to find a formulation for which both the statistical curves and the cone were described well. Besides, the shift of the cone for high incidence angles is to a large extent induced by the asymmetry of the mid beam. The only way in which this could be taken into account is to make the model function beam dependent for this sector.

6 General performance of CMOD5

6.1 cone sections

In Figures 19 to 21, and Figure 18, cones sections of CMOD4 and CMOD5 are compared with the data cone. The cone for CMOD5(KNMI) is not shown, since it is almost identical to that of CMOD4. As can be seen, the position in the vertical for low incidence angles has improved considerably. It is a result of the adaptation of $B0$ for low incidence angles. For high winds, the size and position of the CMOD5 cone is correct for all nodes.

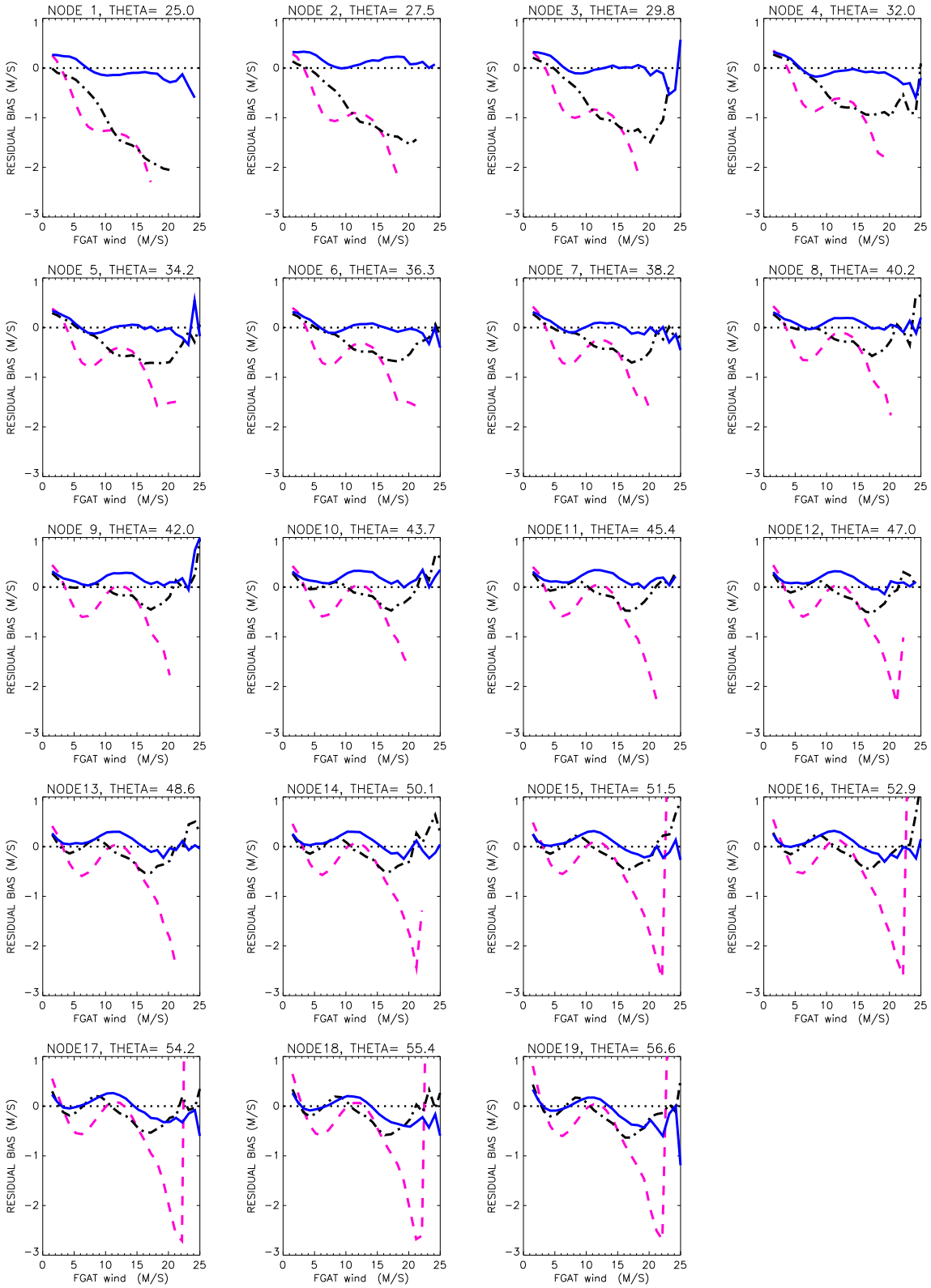

Figure 16: Residual wind biases, as defined in Eq.(17) for CMOD4 (dashed purple), CMOD5(KNMI) (dot-dashed black) and CMOD5 (solid blue).

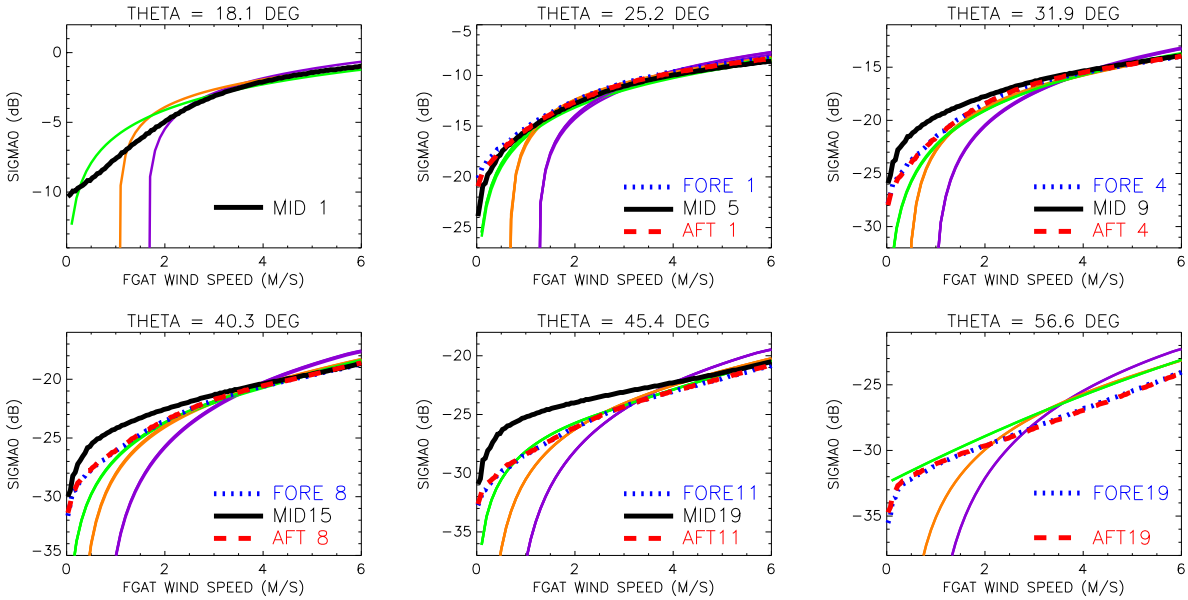

Figure 17: Backscatter based on the statistical method for several incidence angles for the fore (dotted blue), mid (solid black) and aft beam (dashed red). The low-wind behavior of B0 for CMOD4 (purple), CMOD5(KNMI) (beige) and CMOD5 (green) is plotted as well.

The improvement w.r.t. CMOD4 is especially evident for higher nodes, which is the result of a smaller $B2$. For several cases, the double loop structure of the data is well described by the CMOD5 cone. Examples are node 3 for $z_0 = 0.5$ and node 5 for $z_0 = 0.39$. This agreement gives confidence in the correctness of the description for $B1$. Finally, it should be noted that there are still some deviations. As discussed in the previous Section, the discrepancy at low winds is induced by the asymmetry of the mid beam. In addition, for node 5 to 11, the CMOD5 cone is still positioned somewhat too high for winds around 12 $\mathrm{m\,s^{-1}}$. The general picture, however, is quite encouraging.

6.2 Average wind bias and standard deviation

In Figure 16, a detailed picture of the wind-speed behavior of CMOD5, w.r.t. FGAT winds was given. Usually, only average values for these OBS-FGAT quantities are calculated. An example is presented in Figure 22, which shows node-wise averages of the OBS-FGAT bias (left panel) and standard deviation (middle panel). Note that the in Figure 22 presented quantities are mainly determined for those wind speeds that are most common. For the period between September-December 1998, the 10, 50 and 90 percentiles of the global FGAT winds were 3.1, 6.7, resp. 11.0 $\mathrm{m\,s^{-1}}$. Therefore, these averages are hardly sensitive to the CMOD performance at strong winds.

Indeed, the large negative biases for CMOD4 and the node-dependent bias for CMOD5(KNMI) have been removed. The residual bias of CMOD5 is within 0.15 $\mathrm{m\,s^{-1}}$, and on average slightly positive (0.03 $\mathrm{m\,s^{-1}}$). The standard deviation of CMOD5 winds is for the first three nodes comparable to that of CMOD4, around node 5 up to 0.03 $\mathrm{m\,s^{-1}}$ lower, and from node 9 to 19 up to 0.02$\mathrm{m\,s^{-1}}$ higher. Averaged over all nodes, the difference in standard deviation is small. The highest standard deviation of CMOD5 (node 18, 19) is comparable to the highest standard deviation of CMOD4. However, the lowest standard deviation for CMOD5 (node 4) is 0.03$\mathrm{m\,s^{-1}}$ lower than the lowest standard deviation for CMOD4.

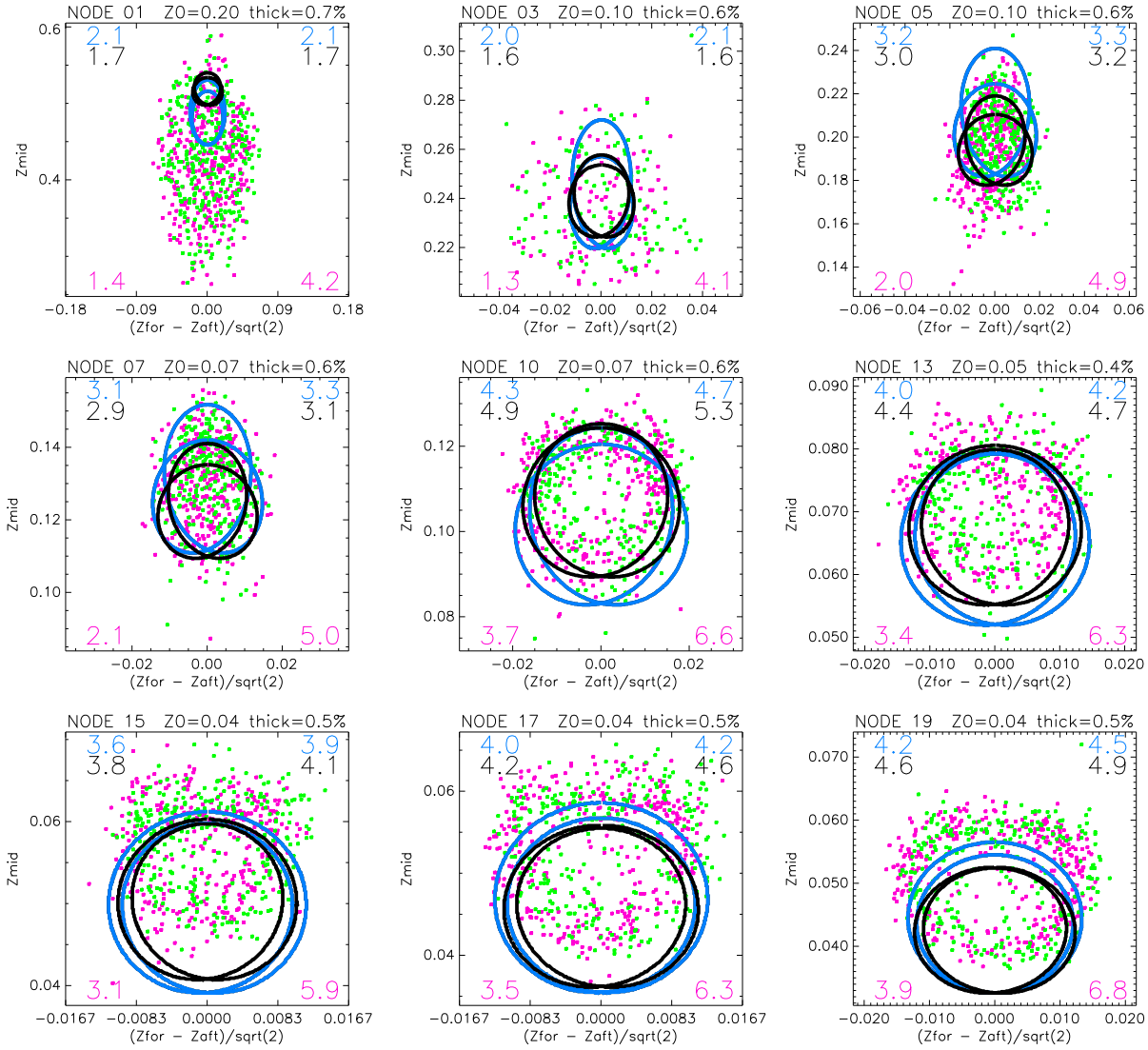

Figure 18: Cone slices for values of z_0 that corresponds to low wind speeds, for nine nodes. Blue curves are cuts of the CMOD4 cone, black curves for CMOD5. Purple points are observed triplets for which the relative wind direction w.r.t. the mid-beam azimuth angle of collocated FGAT winds was between 0 and 180 degrees, green points for directions between 180 and 360 degrees. Numbers within the panels indicate average wind speed plus and minus one standard deviation (left, right resp.) for CMOD4 (blue), CMOD5 (black) and collocated FGAT winds (purple).

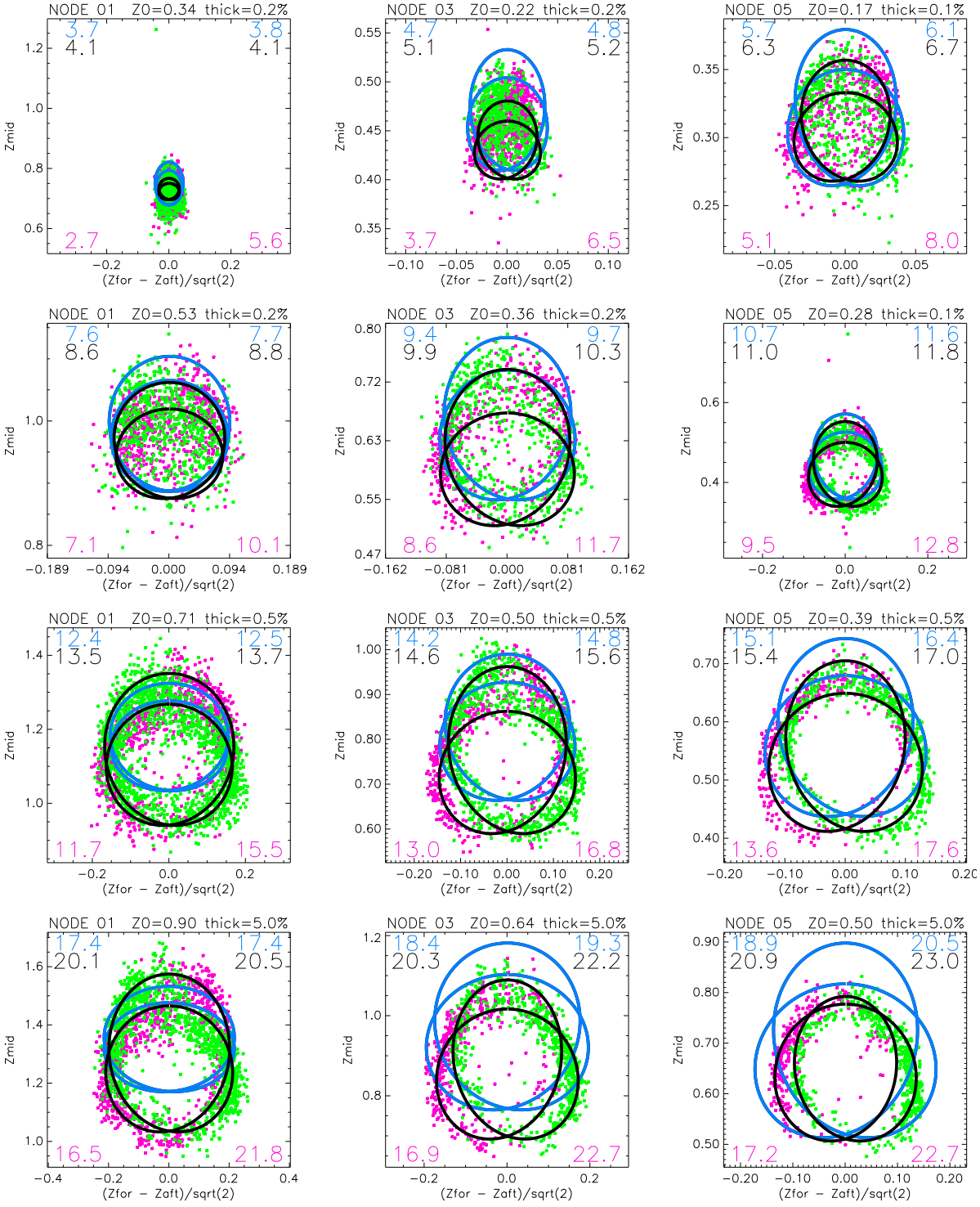

Figure 19: Cone slices for nodes 1, 3 and 5 for several values of z_0. Curves, color coding and numbers are as defined in Figure 18.

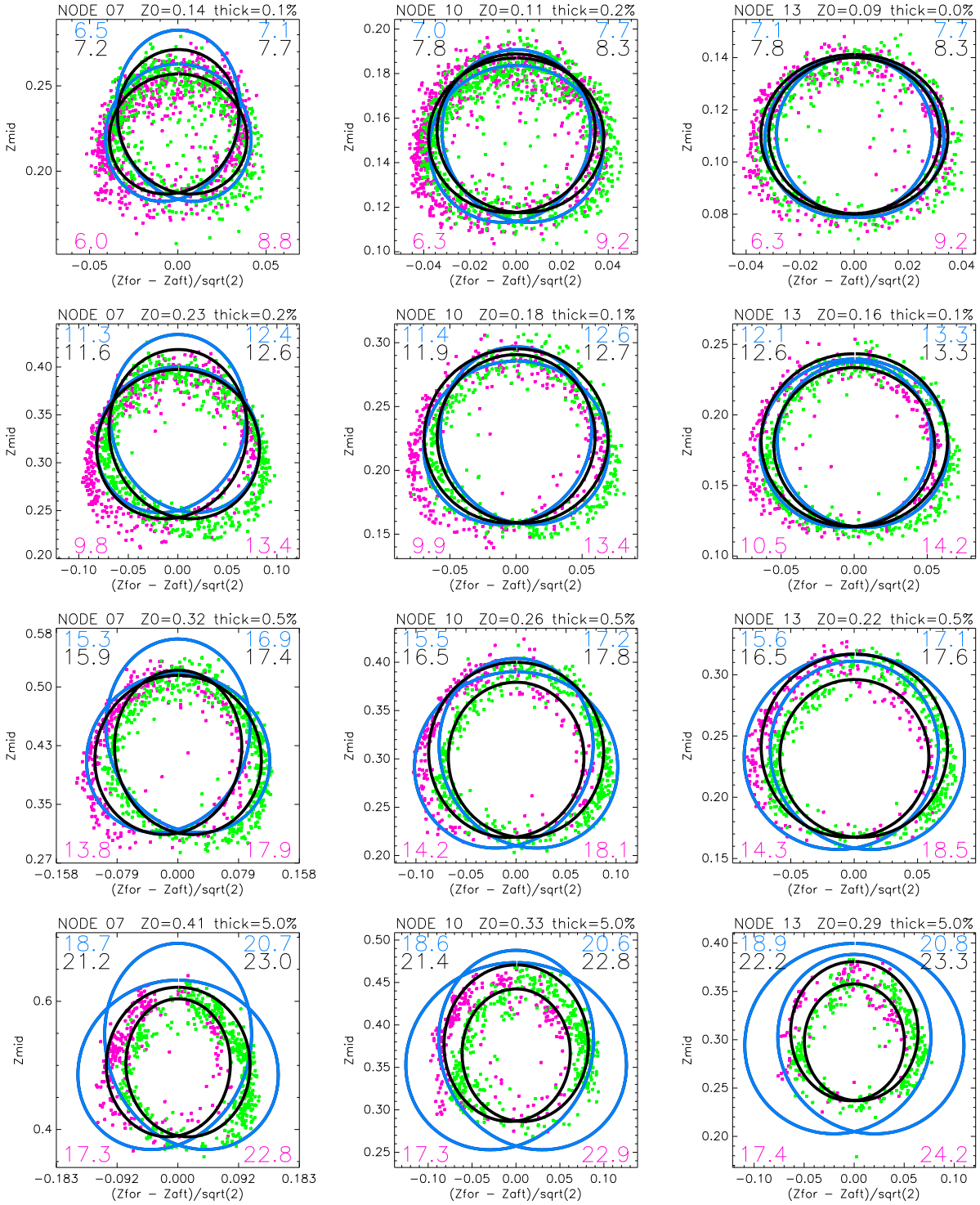

Figure 20: The same as Figure 19, but now for nodes 7, 10 and 13.

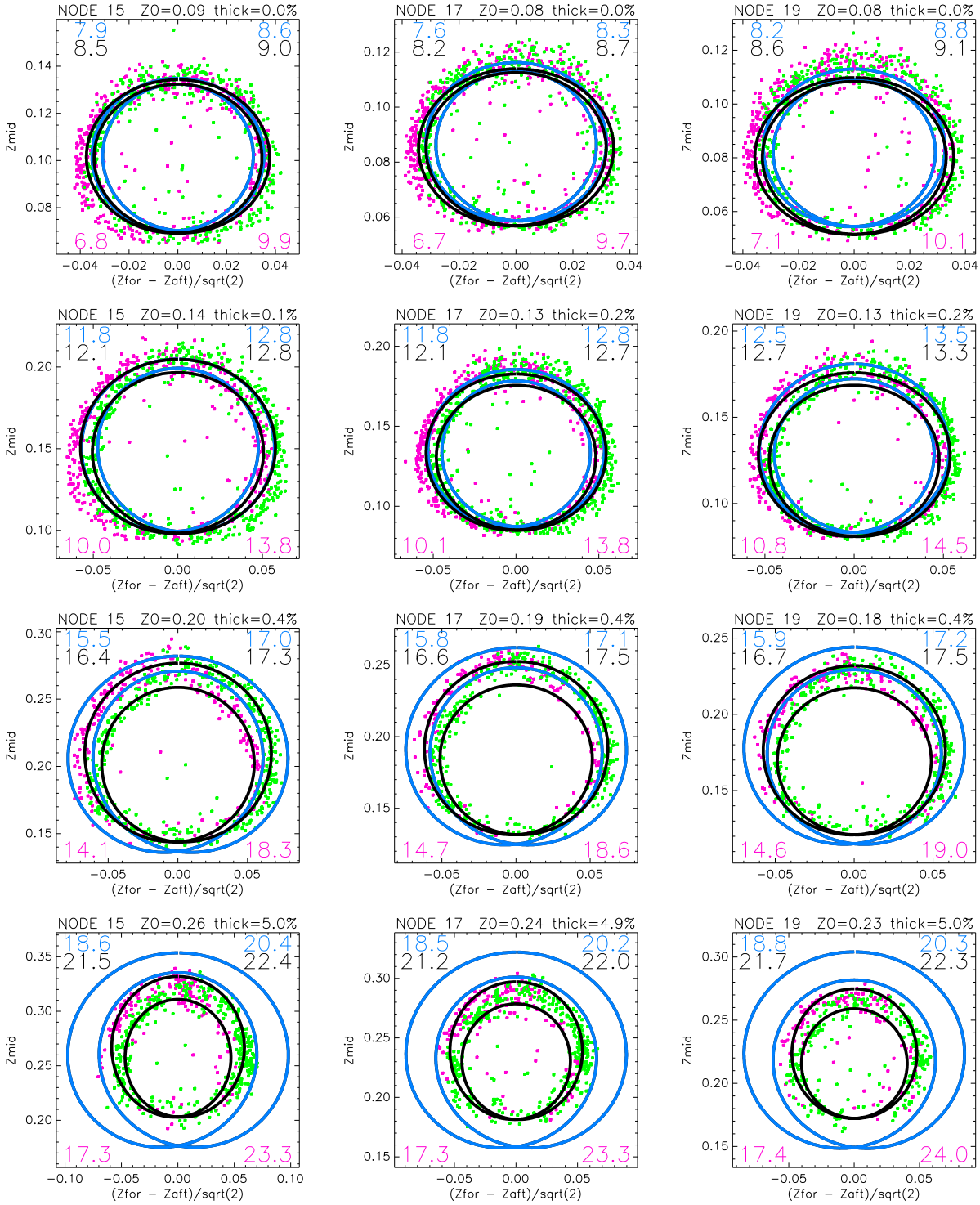

Figure 21: The same as Figure 19, but now for nodes 15, 17 and 19.

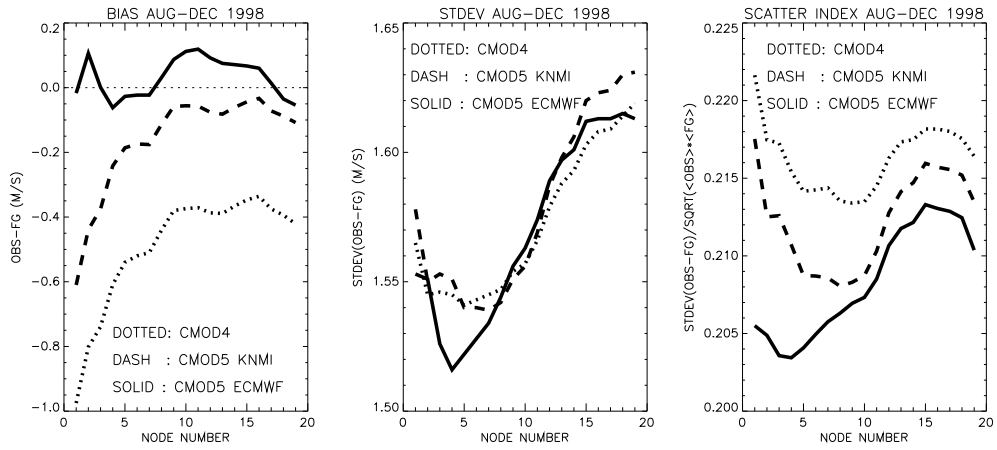

Figure 22: Wind-speed averaged bias, standard deviation and scatter index of inverted winds w.r.t FGAT winds, as a function of node number. Dotted curves are for CMOD4, dashed for CMOD5(KNMI) and solid for CMOD5.

It should be noted that a smaller standard deviation not necessarily induces that the quality of the product is higher. To give an example, it is known that the comparison between CMOD4 winds and FGAT winds improves when the former are enhanced by 5%. It reduces the negative bias. However, the standard deviation of the CMOD4 winds will rise by 5% as well. So, although this operation improves performance, the standard deviation becomes worse. A quantity that corrects for this effect and its misinterpretation is the scatter index (*SI*). It is defined as the standard deviation normalized by the average wind speed:

$$SI = \sqrt{\frac{<(OBS-FGAT)^2> - <OBS-FGAT>^2}{<OBS><FGAT>}}. \tag{20}$$

The value of this dimensionless quantity gives a better view on the intrinsic quality of the wind product. It is displayed in the right panel of Figure 22. The scatter index is lowest for CMOD5 for all nodes. Apparently the lower (OBS-FGAT) standard deviations for CMOD4 at higher nodes are the result from the fact that these winds are too low. After the proper rescaling, standard deviations will increase and become larger than the corresponding standard deviations for CMOD5.

6.3 Ocean calibration

A standard method to detect a drift in the behavior of the three antennas is the ocean calibration (Stoffelen, 1999). For each node and beam it calculates the difference between the average backscatter level measured by the antennas and, based on FGAT winds, the average backscatter level simulated by a CMOD function:

$$O(\theta,\text{beam}) = <z(\text{node}(\theta),\text{beam})> / <z(\text{CMOD}(\theta,\text{FGAT})>. \tag{21}$$

The simulated backscatter values correct for possible seasonal variations of average backscatter measurements induced by differences in wind climate (in the SH winter, winds are stronger than in the NH winter). Therefore, a drift in these 'ocean calibrated' values are connected to real drifts in the antenna behavior (assuming that there is no change in quality of the FGAT winds). The value of the ocean calibration depends on the model function under consideration. If a model function is capable of generating winds that are in line with the FGAT winds, it should also be able give a fair representation of backscatter measurements, given the FGAT winds. Therefore,

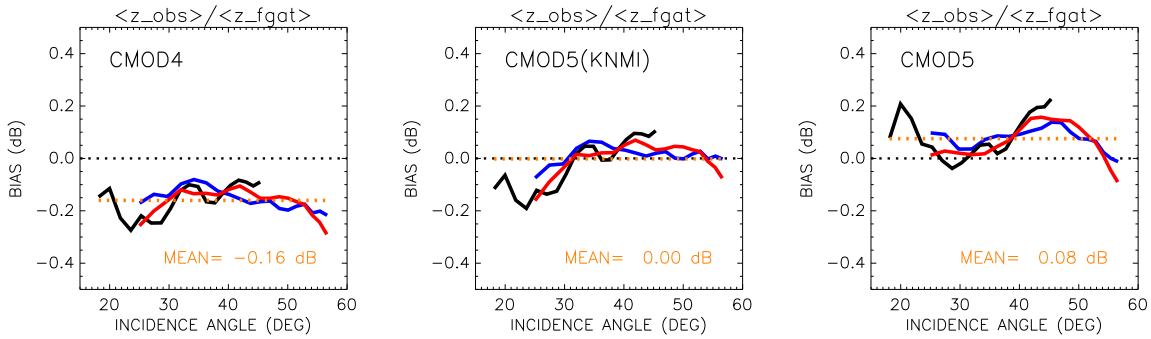

Figure 23: Ocean calibration for fore (blue), mid (black) and aft (red) beam based on CMOD4 (left panel), CMOD5(KNMI) (middle panel) and CMOD5 (right panel).

O should be close to zero, although, due to nonlinearities in the wind-inversion scheme, small deviations from zero may be expected. Large deviations from zero indicate a bias of the winds inverted by the model function under consideration. Typically, relative biases of 0.2 dB are associated with relative wind biases of 0.5 $\mathrm{m\,s^{-1}}$.

In Figure 23, ocean calibration (21) is displayed for CMOD4, CMOD5(KNMI) and CMOD5. In order to eliminate differences due to differences in azimuth angle of the beams, averages are calculated on the basis of the weight function introduced in Section 5.1.1. Levels are lowest for CMOD4, which has the largest negative wind biases. The node-dependent bias of CMOD5(KNMI) winds is reflected by an incidence-angle dependent ocean calibration. For CMOD5, the ocean calibration is more evenly distributed around its average. Although, fluctuations in the ocean calibration values do correspond with fluctuations in the wind bias (see left panel of Figure 22). For CMOD4, such a similarity is less obvious. The average value of the ocean calibration is positive for CMOD5 (0.08 dB). Apparently this value gives rise to nearly unbiased winds (0.03 $\mathrm{m\,s^{-1}}$). It does not need to be exactly zero, for its exact value depends on how the averaging is performed. If, for instance, first averages of σ_0 are calculated, before the transformation to z is made (see Eq. (2)), all values for O were found to decrease with 0.02 dB.

The asymmetry of the mid beam at high incidence angle only gives rise to a relatively small asymmetry in the ocean calibration. The reason that the difference between the curves is not larger is that the ocean calibration is based on the backscatter values (z), which are for high winds much higher than for lower winds. Since the asymmetry is mainly present for winds up to 5 $\mathrm{m\,s^{-1}}$, see e.g. Figure 10, its contribution to the ocean calibration is overshadowed by the symmetric behavior at higher winds with much stronger backscatter values. The difference would have been evident, if averages in Eq. (21) would have been based on dB values instead.

6.4 Scatter plots

Scatter plots of CMOD5 winds versus FGAT winds are presented in Figure 24. From this it is seen that, averaged over all nodes, the agreement between the average values of the CMOD5 winds and FGAT winds is quite good for all wind speeds. The 45-degree line is almost exactly in between the two lines defined by averaging over FGAT winds (Eq. (12)) resp. averaging over CMOD5 winds (Eq. (13)). The negative biases for low nodes are removed. For higher nodes there is a small residual wind-speed dependent bias. This bias can also be seen from Figure (16).

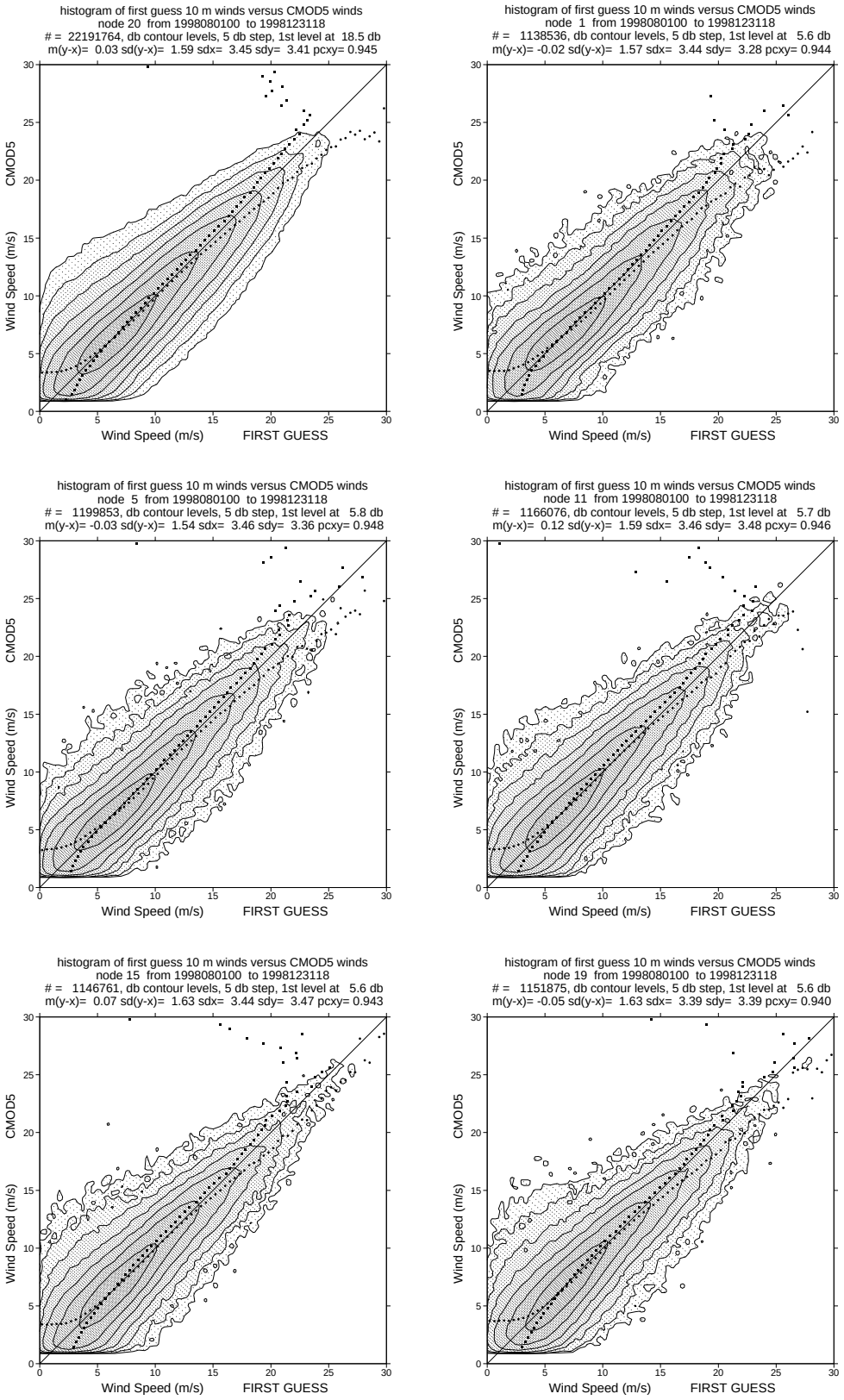

Figure 24: Scatter plot between de-aliased CMOD5 winds and ECMWF FGAT winds for all nodes, and nodes 1, 5, 10, 15 and 19.

6.5 Distance to the cone and rank-1 performance

The quality of $B0$ is to a large extent reflected by the quality of scatter plots between the CMOD winds and FGAT winds. The extent to which the model function cone matches the data cloud, gives an indication for the correctness of $B1$ and $B2$. The typical deviation of a backscatter triplet from the model cone is called the distance to the cone. Its value is defined as the square root of the minimum of Eq. (3), and is returned by the PRESCAT inversion algorithm. The smaller the distance to the cone, the better the fit of the model cone. Besides its distance, it is also possible to determine whether a data triplet is located inside or outside the cone (Stoffelen 2000, page 83). For the wind solution (v,ϕ), $\mathbf{z}(\mathbf{v},\phi)$ is by definition the point on the cone that is closest to the observed triplet. The center $\mathbf{z}_c$ of the cone in a plane of constant z_0 is approximately given by $B0(v,\phi)$, which, as is easily derived from Eq. (1), is given by:

$$\mathbf{z}_c = \frac{1}{3}\sum_{i=1}^{3}\mathbf{z}(v,\phi+i\frac{2\pi}{3}). \tag{22}$$

If the inner product of the difference between the observed triplet $\mathbf{z}^o$ and $\mathbf{z}$ with the difference $\mathbf{z}-\mathbf{z_c}$ is larger than zero, then the observed triplet is outside the cone; otherwise it is located inside the cone. Average values of this quantity give an indication whether the model cone is locally too large or too small.

A way to test the quality of $B1$ is to look at the performance of the rank 1 winds. The higher the frequency that the rank 1 wind is the proper solution (determined by e.g. comparing to the FGAT winds), the better the double structure of the model cone matches the data. This performance is not only determined by $B1$, however. For instance, if $B2$ is much too large, the solution that is closest to the center of the cone will always be selected, even when $B1$ is correct.

In Figures 25 to 29 for each node and model-function wind speed, the performance of the rank 1 wind is presented (left panels). Also, the average cone distance in case the sign is incorporated (middle panels) or is not included (right panels) are presented in these Figures. Performance of these quantities averaged over all wind speeds (so node-wise) is displayed in the lower panels of Figure 29. From these Figures it is seen that CMOD5 gives a much better rank-1 performance for node 3 to 12. Averages higher than 80% are observed for winds between 15 and 20 $\mathrm{m\,s^{-1}}$. For the other nodes, the rank-1 performance is more comparable to CMOD4 and CMOD5(KNMI) and are even somewhat worse for high winds at high nodes.

Positive values of the signed cone distance indicate that the data is more outside than inside the cone, i.e., the model cone is too small. Negative values show that the model cone is too large. Results are on average best for CMOD5. Especially for the lower nodes for all winds, and for higher nodes for high winds, CMOD5 represents the data cone better. Especially the large negative values for CMOD4 and CMOD5(KNMI) at high winds indicate that these cones are considerably oversized in these regions. The CMOD5 cone fits the data cone much better at this high end of the cone. For winds below 5 $\mathrm{m\,s^{-1}}$ for the higher nodes, however, the signed distance to the cone is worse than that for CMOD4 and CMOD5(KNMI). It must be induced by the displacement of the CMOD5 cone in the mid-beam direction (see e.g. Figure 18). Therefore, the large positive values do not necessary indicate that the CMOD5 cone is too small. In fact, its size seems to be appropriate, as can be seen from the lower panels of Figure 18. Again, this is due to the asymmetry of the mid beam.

For higher nodes the CMOD4 and CMOD5(KNMI) cones are clearly too small for winds between 5 and 15 $\mathrm{m\,s^{-1}}$, while the situation for CMOD5 is much better. Indeed, as can be seen from the lower right panel of Figure 13, this observation was anticipated by the Fourier method. In general a close relationship between a deviation from the Fourier estimate and non-zero values for the signed cone distance was observed, which gives some confidence on the quality of the Fourier method.

The average distance of the cone itself, is presented in the right panels of Figures 25 to 29. For node 1 to 6,

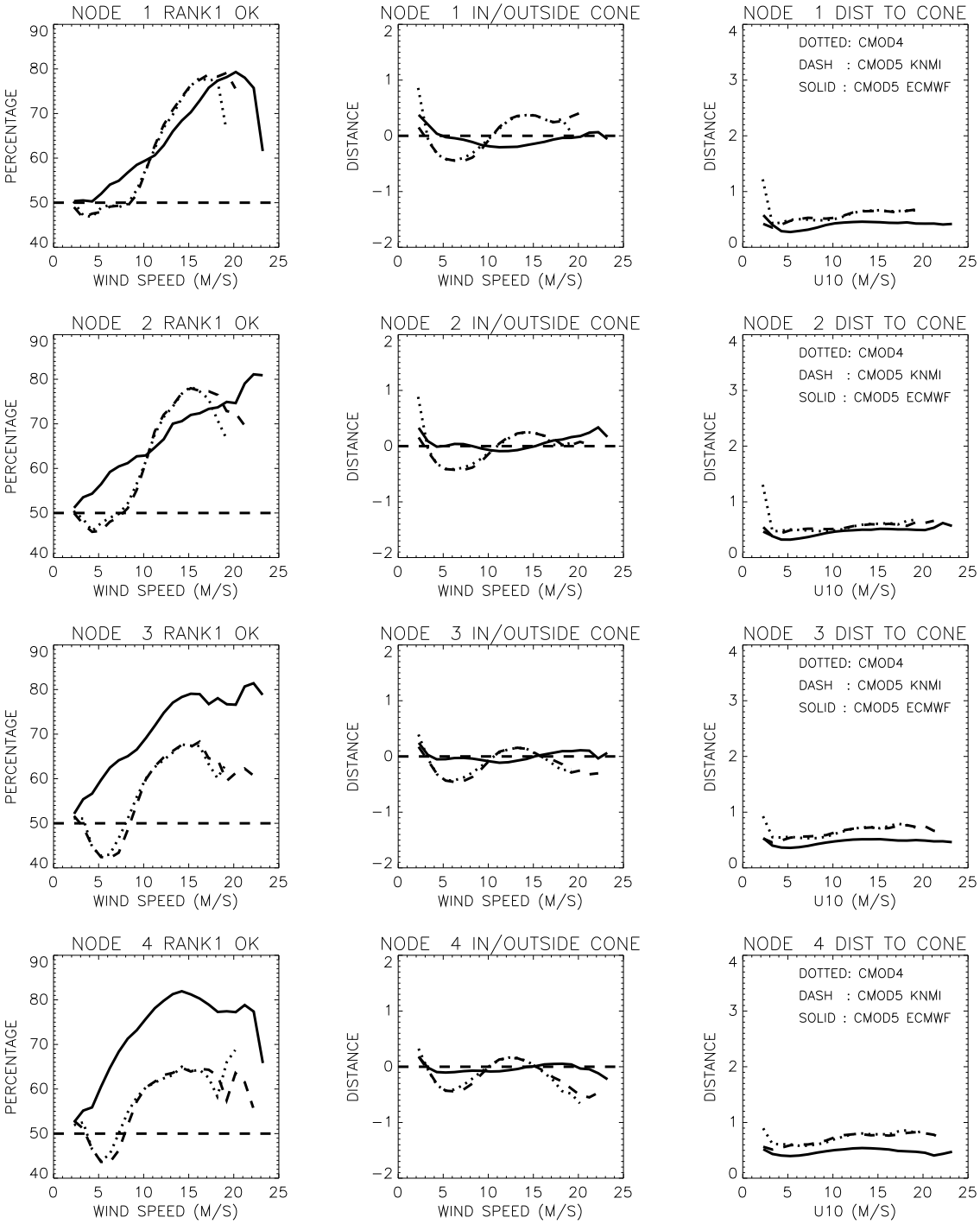

Figure 25: Percentage for which the rank1 solution matches FGAT winds best (left panels), average distance to the cone, including the sign (middle panels) and average distance to the cone (right panels), as function of CMOD wind speed, for node 1 to 4.

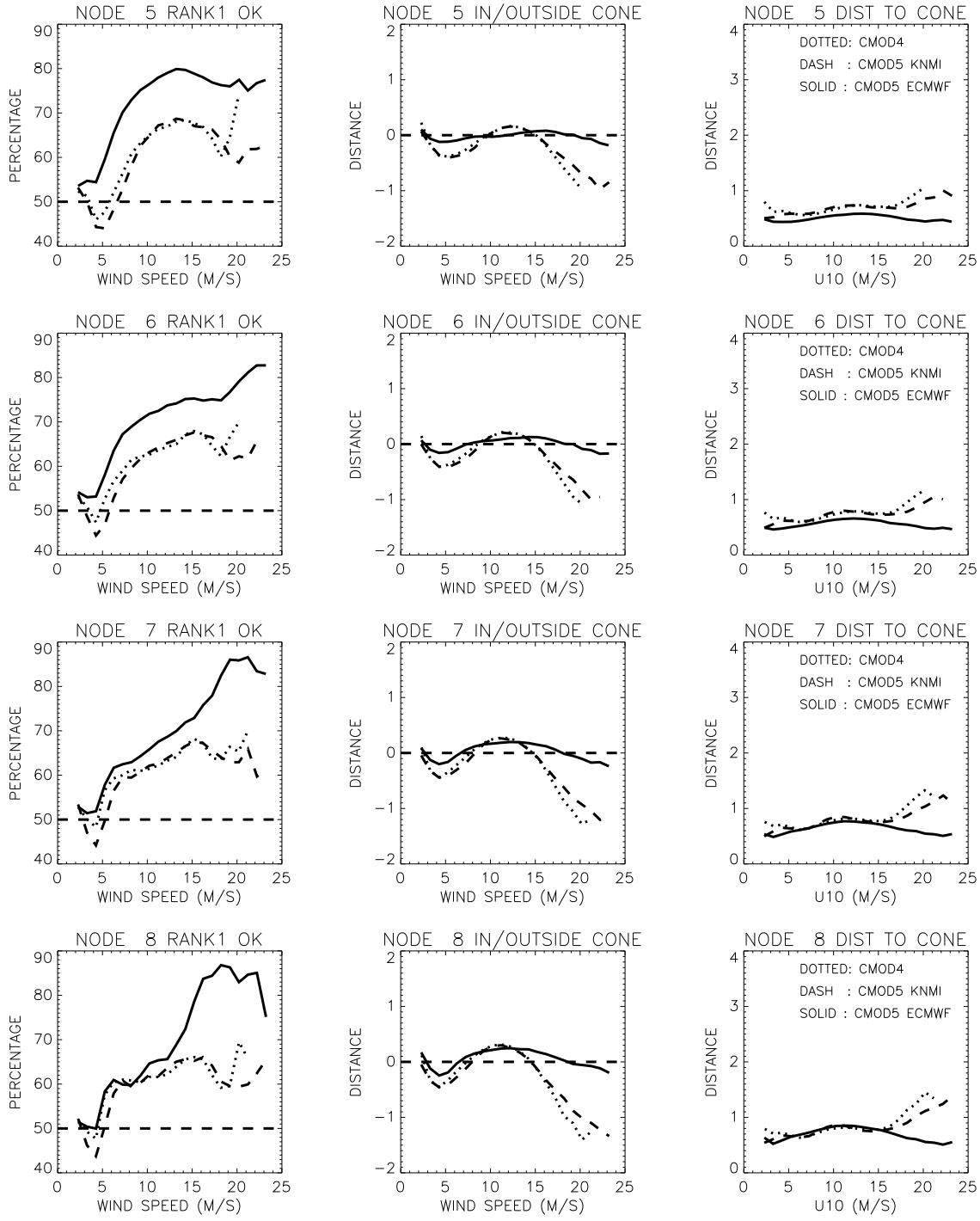

Figure 26: Percentage for which the rank1 solution matches FGAT winds best (left panels), average distance to the cone, including the sign (middle panels) and average distance to the cone (right panels), as function of CMOD wind speed, for node 5 to 7.

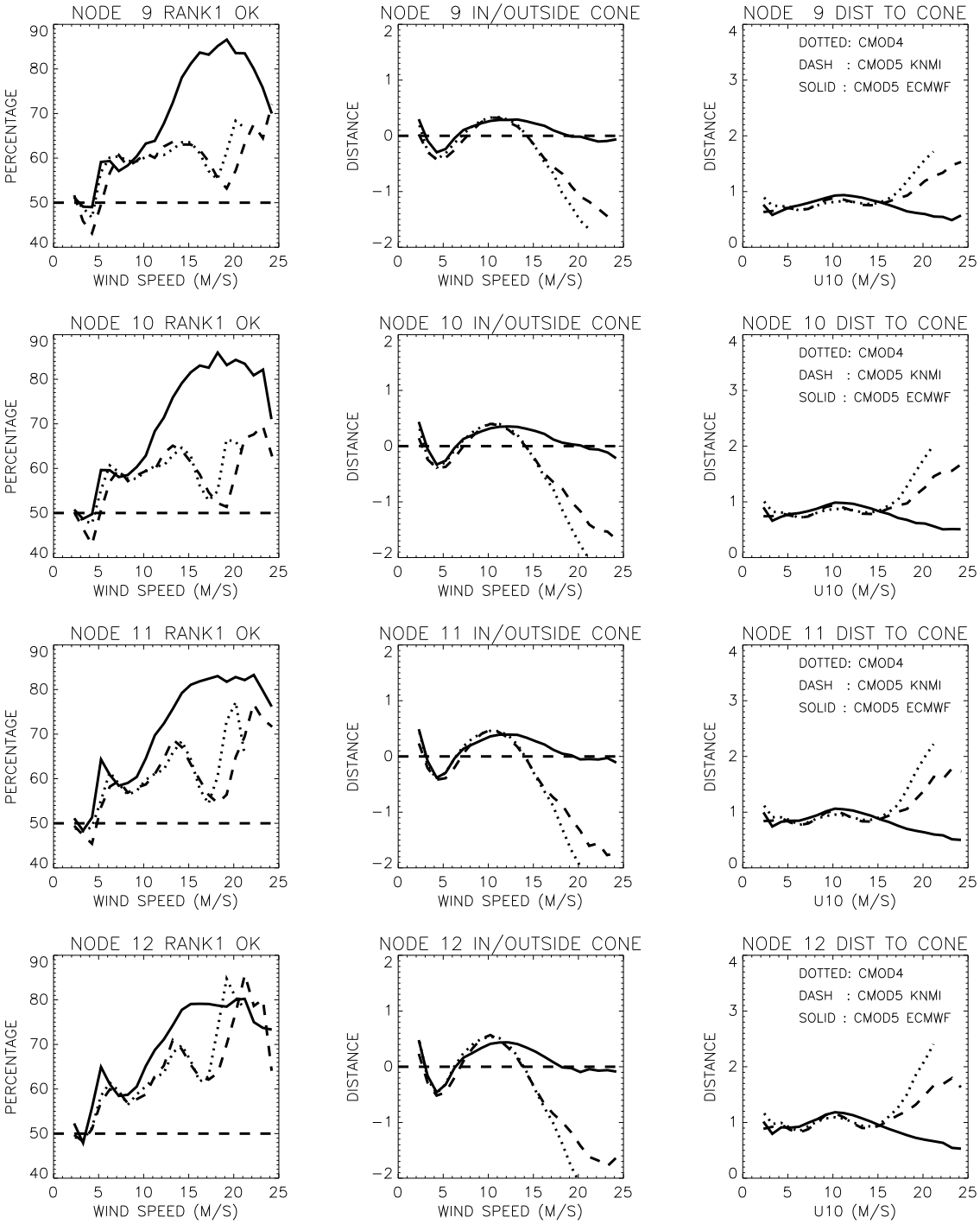

Figure 27: Percentage for which the rank1 solution matches FGAT winds best (left panels), average distance to the cone, including the sign (middle panels) and average distance to the cone (right panels), as function of CMOD wind speed, for node 8 to 11.

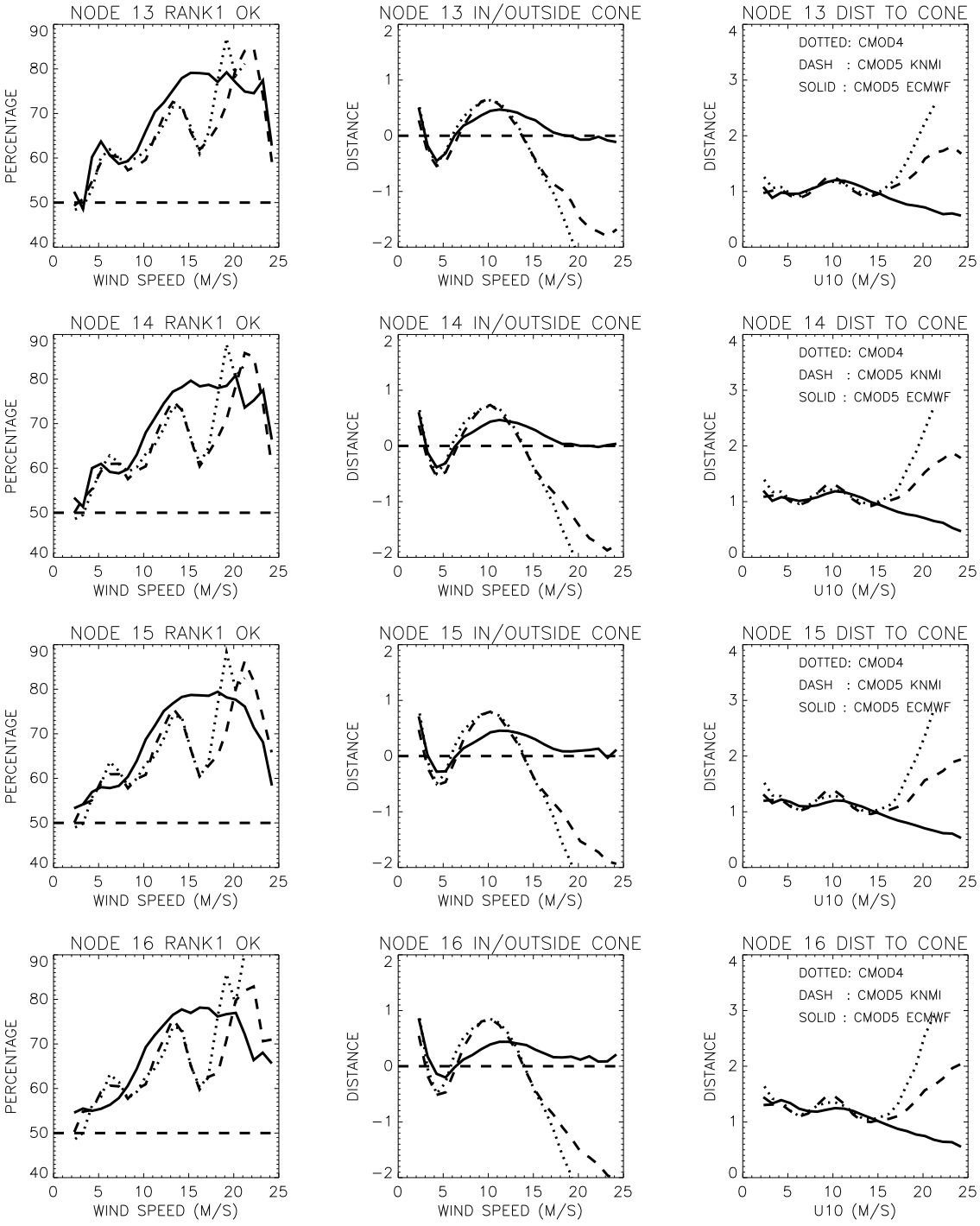

Figure 28: Percentage for which the rank1 solution matches FGAT winds best (left panels), average distance to the cone, including the sign (middle panels) and average distance to the cone (right panels), as function of CMOD wind speed, for node 12 to 15.

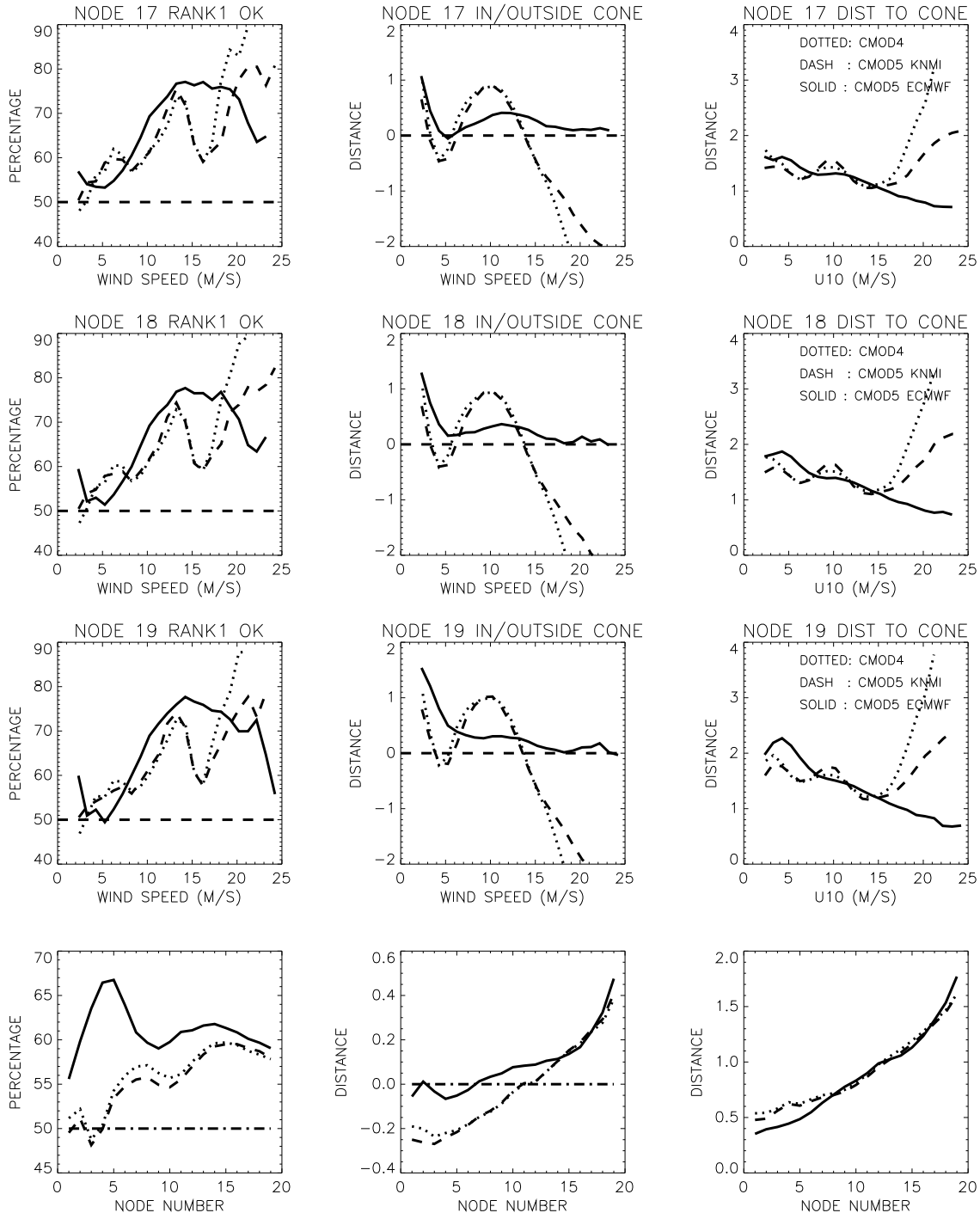

Figure 29: Percentage for which the rank1 solution matches FGAT winds best (left panels), average distance to the cone, including the sign (middle panels) and average distance to the cone (right panels), as function of CMOD wind speed, for node 15 to 19, and as function of node number for the lower panels.

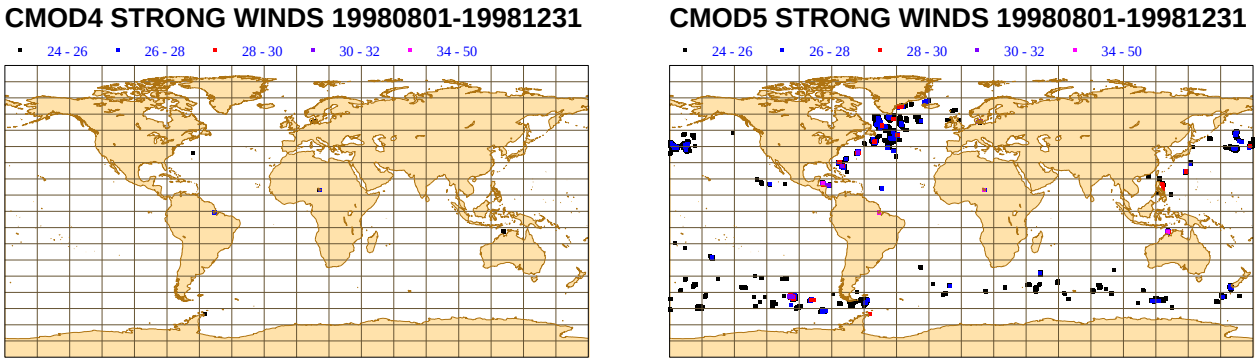

Figure 30: Retrieved ERS-2 winds of 24 ms^{-1} and higher in the period August-December 1998. The left panel shows results for CMOD4 inversion, the right panel for CMOD5.

CMOD5 gives consistently lower values of this distance. For node 7 to 17 the behavior of the three model functions is comparable for winds up to 15 ms^{-1}. For higher winds, CMOD5 gives superior results. Instead of an 'explosive' growth, as is the case for CMOD4 and CMOD5(KNMI), it actually reduces for more extreme winds. The difference between the CMOD4 and CMOD5(KNMI) distances is induced by the fact that stratification was performed w.r.t. inverted winds. Therefore, CMOD4 curves, are for high winds more shifted towards lower winds. For the highest nodes, the CMOD5 cone distance for low winds is worse than for CMOD4 and CMOD5(KNMI). It is induced by the asymmetry of the mid beam.

From the lower panels of Figure 29 node-wise averages are presented. These averages are mainly determined by the most frequent wind speeds, which is in the range between 3 and 11 ms^{-1} (see Section 6.2). This is the reason why for the higher nodes the excellent behavior for large winds is compensated by the worse performance at low winds. For lower nodes, CMOD5 performs better in the complete wind-speed range, and therefore exhibits also a better node-wise averaged behavior.

7 Strong winds

The CMOD5(KNMI) and CMOD5 give a better representation for high winds than CMOD4 does. In Figure 30 all inverted winds of 24 ms^{-1} or larger during the period 1 September to 31 December 1998, are plotted for CMOD4 (top panel) and CMOD5 (lower panel). As can be seen, the difference is striking. Besides the erroneous winds for the Amazon estuary, Lake Tsjaad, Antarctica and Denmark, such high winds were only observed for hurricane Danielle and tropical cyclone Thelma. For CMOD5, on the other hand, for many tropical cyclones and extra-tropical storms, retrieved winds are 24 ms^{-1} or higher. For CMOD5(KNMI) even stronger winds are observed (see Figure 31), especially at higher nodes.

The most extreme wind-situation observed by the ERS-2 satellite in the five-months period was hurricane Mitch. This category 5 hurricane was covered twice. In Figure 32, Mitch is shown for 16:00 UTC 27 October 1998, which was around its maximum intensity. Wind fields are based on CMOD4 (top left), CMOD5 (top right) and CMOD5(KNMI) (lower left panel). De-aliasing is based on the wind solution that represents the circulation around the observed TC center (indicated by cross-wire) best. FGAT winds are shown in the lower right panel. As can be seen, its circulation is displaced w.r.t. the observed location. Besides, its maximum winds (25 knots) are much lower than observed peak values of 155 knots. For CMOD4 maximum winds are 45 knots, for CMOD5 this is 70 knots, while based on CMOD5(KNMI), winds up to 80 knots are observed. For CMOD4, the wind directions are quite noisy near the TC location, while the CMOD5(KNMI) winds look to be

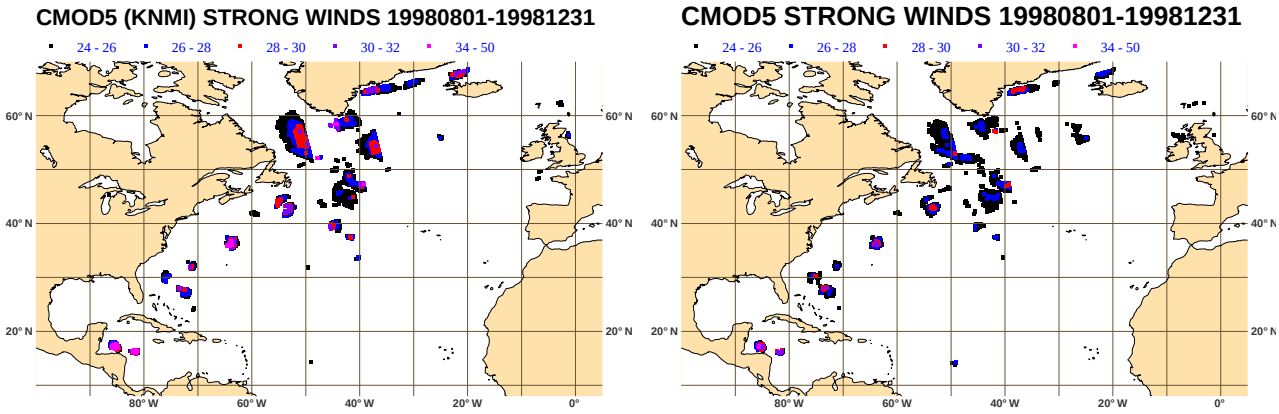

Figure 31: Retrieved ERS-2 winds of 24 ms^{-1} and higher in the period August-December 1998. The left panel shows results for CMOD5(KNMI) inversion, the right panel for CMOD5.

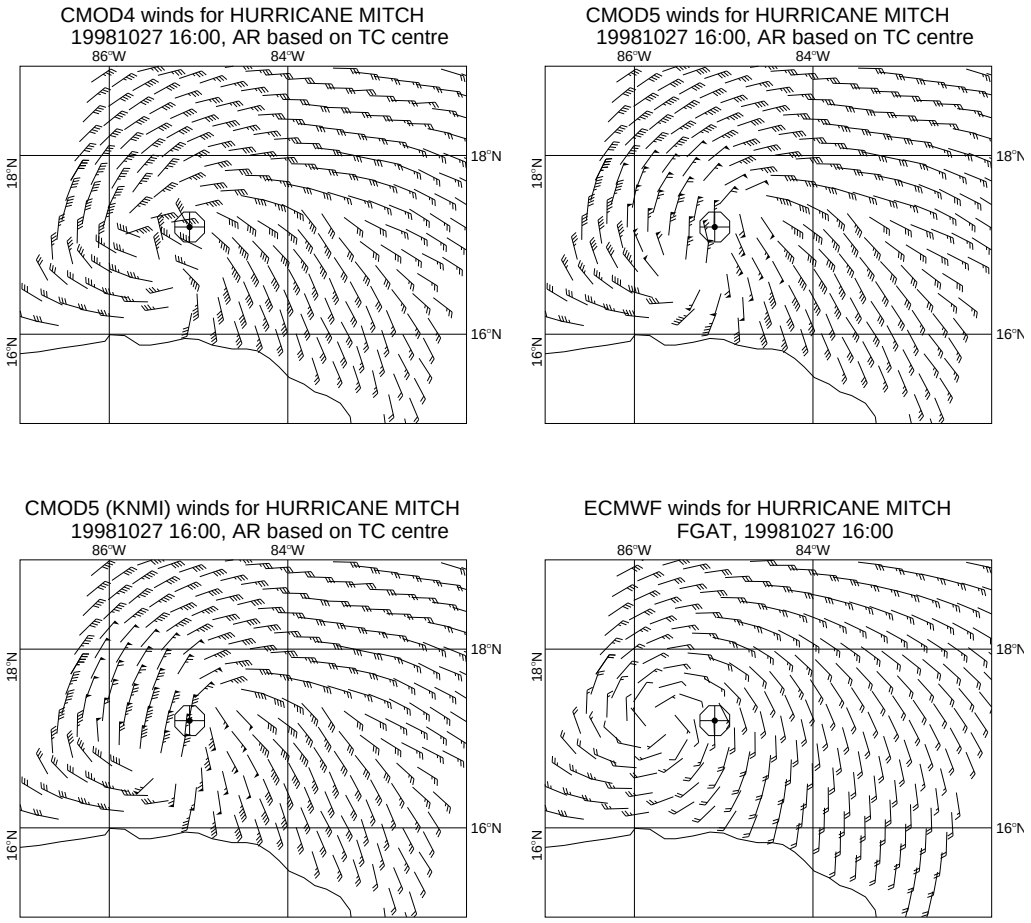

Figure 32: Hurricane Mitch near its maximum strength for CMOD4 winds (top left), CMOD5 winds (top right), CMOD5(KNMI) winds (bottom left) and FGAT winds (bottom right).

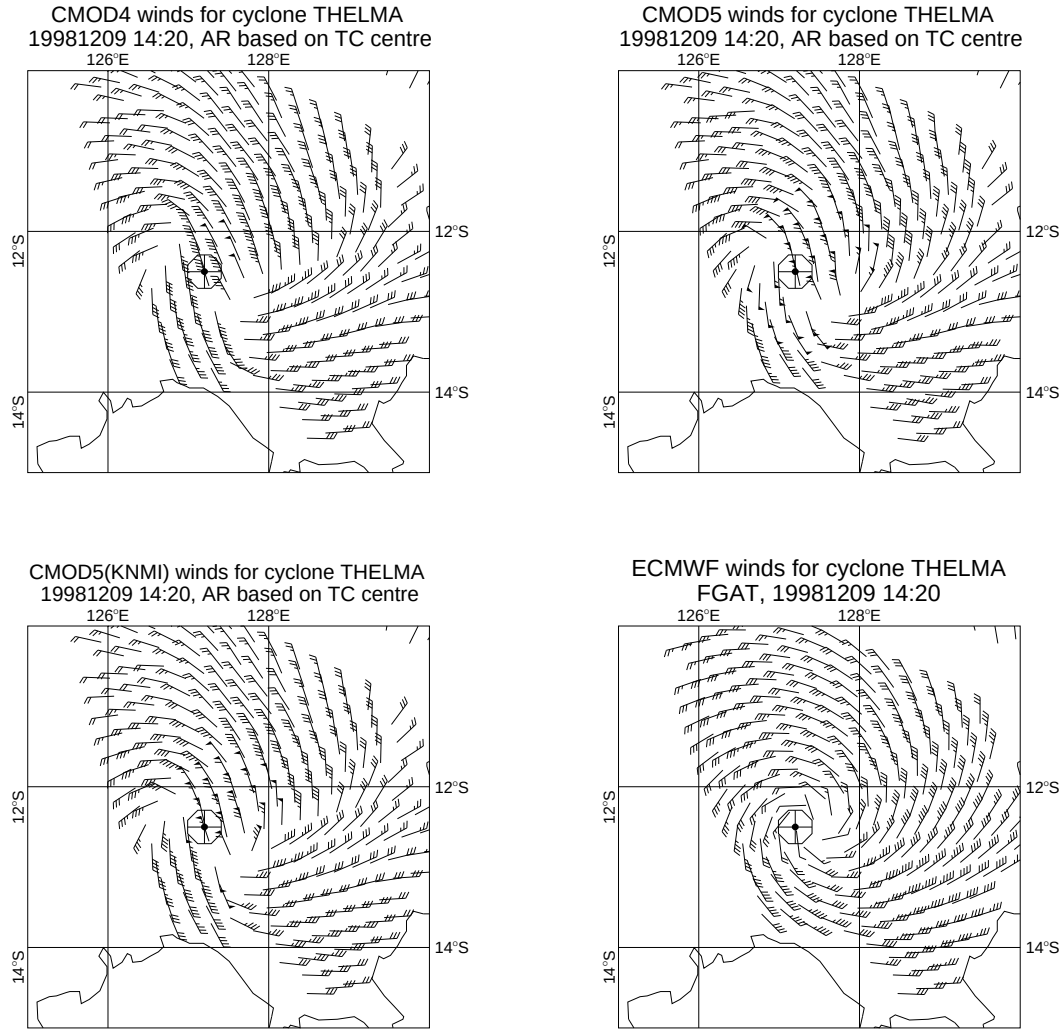

Figure 33: Tropical cyclone for CMOD4 winds (top left), CMOD5 winds (top right), CMOD5(KNMI) winds (bottom left) and FGAT winds (bottom right).

grouped into patches of similar wind directions. The most continuous direction distribution is obtained by the CMOD5 model function.

A second example of an extreme case is given in Figure 33. It concerns TC Thelma at 14:20 UTC 9 December 1998. Wind fields are plotted as for Figure 32. The FGAT field matches the TC center well, and maximum wind speeds of 45 knots give a better representation than it was the case for Mitch. Maximum CMOD4 winds are 50 knots, CMOD5 winds 70 knots, and CMOD5(KNMI) winds 75 knots. The reason why the difference between the CMOD5 winds and CMOD5(KNMI) winds is smaller is because they concern measurements at low incidence angles. The directional structure of the vortex described by CMOD5 is the most realistic one. Both CMOD4 and CMOD5(KNMI) winds are, again, grouped into directional patches.

For tropical cyclones it is obvious that the maximum observed winds are much stronger than the values obtained from the CMOD functions. In that respect, the CMOD5(KNMI) winds give the smallest under-estimation. For extra-tropical storms, however, the CMOD winds are expected to be capable of giving a fair description of the maximally observed winds. For several of such storms, there was a search for independent conventional data

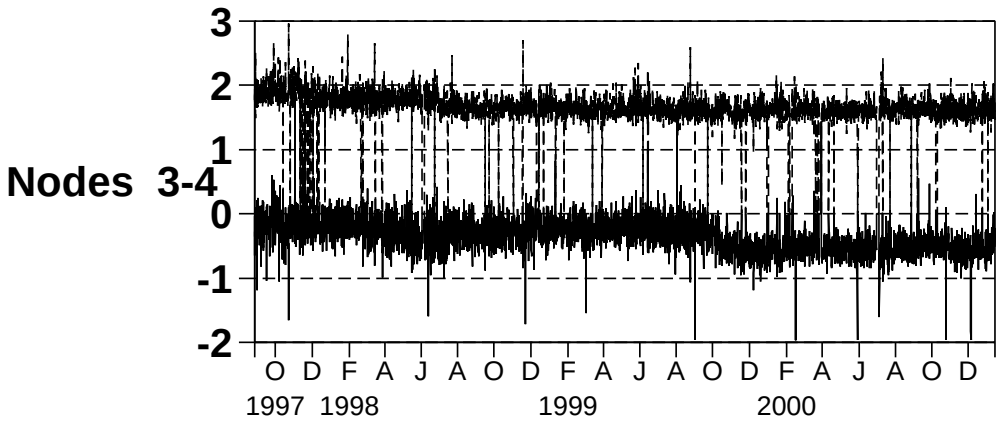

Figure 34: Time series of the difference between the ERS-2 scatterometer winds as used at ECMWF and collocated ECMWF FGAT winds. Shown are bias levels and standard deviations, averaged over all measurements of node 3 and 4 in 6-hourly periods.

sources, in order to assess whether the CMOD5 winds are too low, or the CMOD5(KNMI) winds too strong. However, no such data was found. Apparently ships tend to avoid such adverse weather conditions.

8 Validation for other periods

8.1 Trends between ERS-2 scatterometer winds and ECMWF FGAT winds

In this study, ECMWF FGAT winds for the period between August and December 1998 have been the baseline for the derivation of CMOD5. The formulation and coefficients of CMOD5 have been tuned in such a way, that biases between inverted winds and FGAT winds were minimal. The obvious question may arise what the level of quality of the FGAT winds is in general, and for the considered period in specific. Besides the random error, possible biases w.r.t. to 'true' winds are especially important. A proper answer to this question could be provided by a collocation study with an independent wind data set, such as buoys, altimeter or QuikSCAT winds. Such a method allows for the estimation of random errors of each data set w.r.t. the 'true' winds. However, it will only reveal relative biases between the various data sources. Only after one assumes knowledge of the absolute bias characteristics of one observation type (e.g., buoys), statements on absolute biases can be made. Such a collocation study was beyond the scope of this project. Instead, the evolution of the difference between ERS-2 winds and ECMWF FGAT winds will be discussed here. Changes or trends in such time series will reveal changes in the ECMWF model winds, and/or changes in the scatterometer characteristics.

Figure 34 shows the evolution of ERS-2 scatterometer obs-background departures and their standard deviation for the period between September 1997 and January 2001. Shown are averages over 6-hourly data batches for nodes 3 and 4. For other nodes time series are very similar. During the entire period shown in Figure 34, ERS-2 scatterometer winds were used in the operational ECMWF assimilation system (LeMeur *et al.* 1997). Instead of assimilating CMOD4 winds directly, backscatter values were bias corrected, before presented to the PRESCAT code. After inversion, additional wind bias corrections were applied as well. These 'ECMOD' winds have not been discussed in this paper so far. Reason for this is that the standard deviations for these winds are between 0.1 and 0.25 $\mathrm{m\,s^{-1}}$ higher than that of the pure CMOD4 winds (results not shown). Scatter indices are higher as well. Clearly, they are not optimal. For all node numbers, the ECMOD winds are on average 0.2 $\mathrm{m\,s^{-1}}$ lower

than the CMOD5 winds. For strong winds, the ECMOD winds do not show the saturation behavior of CMOD4 winds and are more comparable to the FGAT, CMOD5(KNMI) and CMOD5 winds.

From Figure 34 three rather abrupt changes can be seen. They are related to model upgrades. In corresponding time series for ERA40 (not shown), these changes are absent. From the list of changes within each of these three model upgrades, the for the surface winds most important changes were:

- 25 November 1997. Introduction of the 4D-Var assimilation system (Rabier *et al.* 2000). The standard deviation between ECMOD and FGAT winds is reduced.
- 29 June 1998. The atmospheric model and ocean wave model are two-way coupled (Janssen *et al.* 2002). The standard deviation between ECMOD and FGAT winds is further reduced.
- 12 October 1999. The number of vertical model levels is increased from 50 to 60 (Teixeira, 1999), and the observation operator for surface winds was changed. The introduction of the assimilation of SSMI 10m-winds (Gérard and McNally 1999), had the largest impact on winds. On average, FGAT winds increase with 0.24 $\mathrm{m\,s^{-1}}$, leading to a more negative bias between ECMOD and FGAT winds.

The CMOD4, CMOD5(KNMI), CMOD5 and CMODEC winds are all linked to the same backscatter data. Therefore, trends for the ECMOD minus FGAT winds, will also be seen when using a different model function. A more detailed picture of the time evolution of CMOD winds compared to the ECMWF first guess was obtained by inverting winds for the month December in 1997, 1998, 1999 and 2000. The results are presented in Figure 35. From this it is seen that there is an evolution of the bias levels (top panels), standard deviations (middle panels) and scatter indices (lower panels) which is consistent with the evolution of the ECMOD winds (Figure 34). Bias levels for December 1997 and December 1998 are similar, and after the introduction of SSMI surface winds, bias levels are similar for December 1999 and December 2000, though 0.25 $\mathrm{m\,s^{-1}}$ more negative than before its introduction. Standard deviations and scatter indices are worst for December 1997 (for this period the vertical scale of the plots is different from the other three periods). Although this is just after the introduction of 4D-Var, the agreement between CMOD winds and FGAT winds is better than before this model change (results not shown). Highest quality is achieved for December 1999. The somewhat better quality compared to December 1998 may be a result of the introduction of the SSMI winds, and the improvement with respect to December 1997 is induced by the two-way coupling between winds and waves. For December 2000, standard deviations have increased by 0.05 $\mathrm{m\,s^{-1}}$. It is difficult to say whether this is due to a model change, a degradation of the scatterometer, or caused by natural inter-annual variations.

Apart from the evolution of average quantities, relative differences in performance between the three model functions, and between different incidence angles is quite stable. Bias levels are most negative for CMOD4, especially at low incidence angles, and for CMOD5, are nearly independent on node number. Bias levels of CMOD5(KNMI) are in between the levels of CMOD4 and CMOD5. Standard deviations are most optimal for CMOD5 at node 3 or 4. At higher nodes, standard deviations between the three model functions are comparable. The scatter index, finally is best for CMOD5 for all four periods, especially at lower nodes. CMOD5(KNMI) scores in between CMOD4 and CMOD5.

8.2 Trends in the ERS-2 scatterometer backscatter distribution

In the previous section it was argued that trends in the behavior of CMOD winds compared to FGAT winds, were largely accounted for by changes in the ECMWF assimilation system. In this section the attention will be focused on backscatter space, which allows for a more accurate determination of trends in the inter-beam consistency of the ERS-2 scatterometer. Two methods that are suitable for this are ocean calibration (Section 6.3)

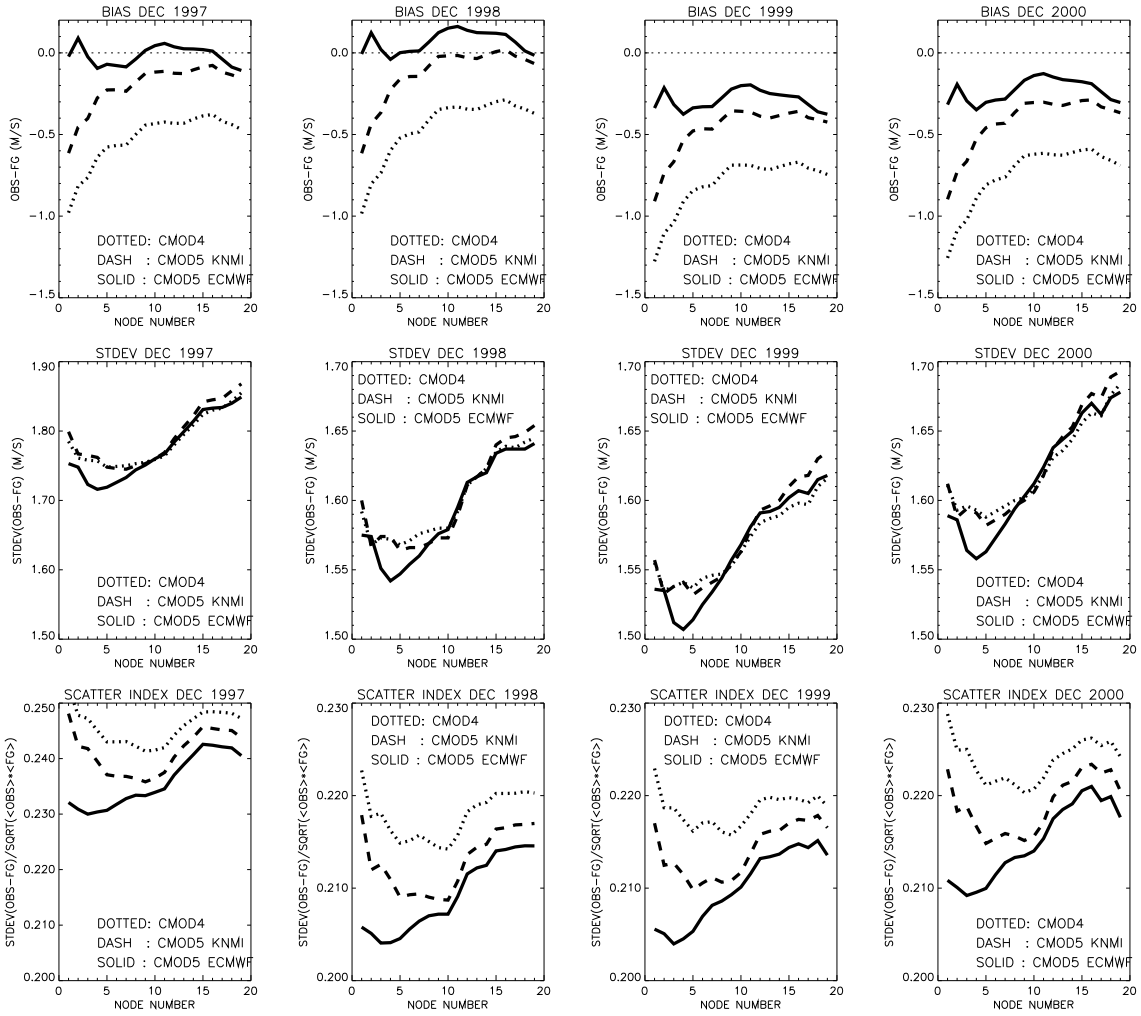

Figure 35: Node-wise averages of bias, standard deviation and scatter index between CMOD winds and ECMWF FGAT winds for the indicated periods. Dotted curves are for CMOD4 inverted winds, dashed curves for CMOD5(KNMI) and solid curves for CMOD5.

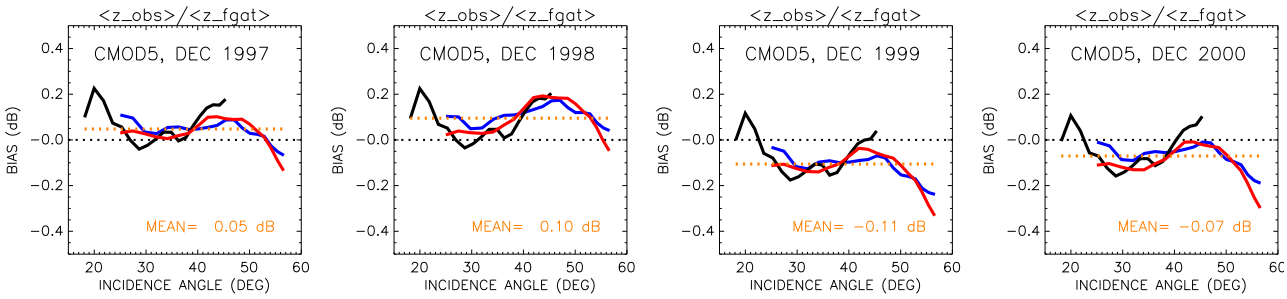

Figure 36: Ocean calibration based on CMOD5 winds for December 1997, 1998, 1999 and 2000.

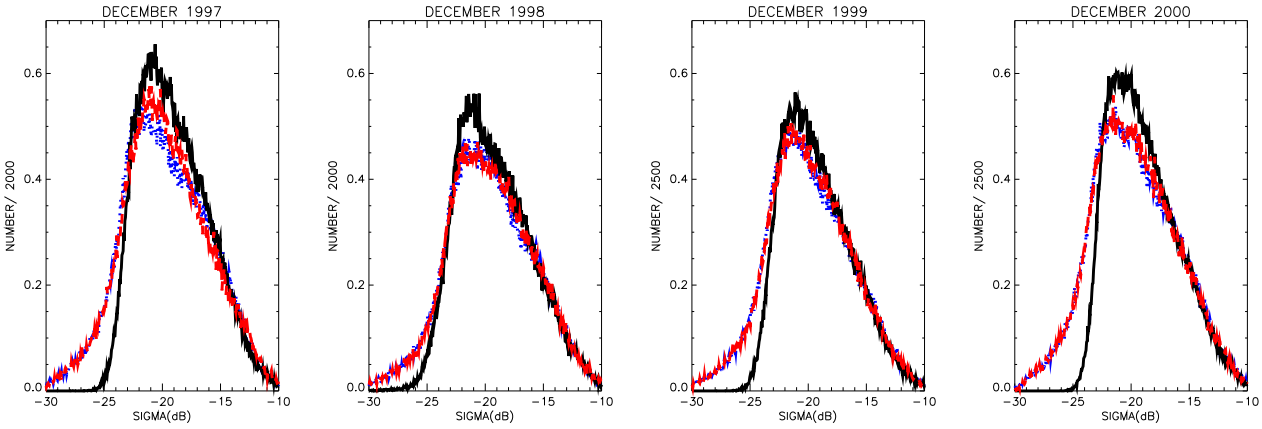

Figure 37: Distribution of backscatter values of the node 19 mid beam (black curves) and the node 11 fore (blue curves) and aft (red curves). Averages are for December 1997, 1998, 1999 and 2000.

and the plotting of backscatter distributions. In Figure 36 the ocean calibration based on CMOD5 (see Eq. 21) is shown for the periods December 1997, 1998, 1999, and 2000. Results based on CMOD4 and CMOD5(KNMI) are linked to these plots in a similar way as they were in Figure 23. They will not be discussed here. The trend in average levels corresponds to the trends in wind speeds discussed in the previous section. Besides these trends, the inter-beam agreement is quite good and more or a less constant over time. Note that the asymmetry of the mid beam at high incidence angle (45.4 degrees) as it was observed for the period August to December 1998 (see right panel of Figure 23) is hardly present for the period of December of that year. However, the asymmetry is visible for the other December months considered, and is most prominent for December 2000. The asymmetry is best observed when plotting the full backscatter distribution of the three beams at this incidence angle (like it was done at the lower right panel of Figure 10). The result is shown in Figure 37. It clearly shows the underflow problem of the mid beam. As the ocean calibration suggested, it is least prominent, though clearly present, for December 1998. For the other periods there are hardly any mid beam backscatter values below -25 dB, which is 5 dB (i.e., a factor of 3) higher than the lowest fore and aft backscatter measurements.

9 Conclusion and discussion

A new model function for C-band scatterometry has been developed on the basis of a comparison of observed backscatter triplets with collocated ECMWF FGAT winds for the period from August to December 1998. Its functional form was redesigned from scratch, and depends on 28 coefficients. In its definition it was tried to retain maximum flexibility, such that possibly future adaptations can be incorporated by an update of the coefficients only, without requiring a redefinition of the functional form.

In backscatter space, the CMOD5 cone corresponds in general much better to the cloud of observed triplets, than the corresponding cones defined by CMOD4 and CMOD5(KNMI) do. The model cone is to a large extent determined by the $B1$ and $B2$ terms. Especially for strong winds, the correct reduction of the model cone diameter, is the result of a proper redefinition of the $B2$ term. In addition, for several cuts of the cone, a double loop structure observed in the data, is correctly described by the CMOD5 formulation. It is the result of a proper redefinition of the $B1$ term. For low incidence angles at high backscatter values (i.e., strong winds) a shift in the mid-beam direction of the CMOD4 and CMOD5(KNMI) cone w.r.t. to the data cone has been corrected. It is the result of an improved description of the variation of the $B0$ term as function of (low) incidence angle. The distance to the cone, which is a measure to what degree the model cone is able to describe the data cloud,

is in general lowest for CMOD5. Especially, towards strong winds the CMOD5 distance to the cone decreases while it rapidly increases for CMOD4 and CMOD5(KNMI).

Only for high incidence angles at low wind speeds CMOD5 is not optimal. The CMOD5 model cone is, compared to the data, more misplaced in the mid-beam direction than the other two model cones are. Also, for this combination of incidence angle and wind speed, the distance to the cone is largest for CMOD5. A reason for this non-optimal behavior is an asymmetry between the mid beam when compared to the fore and aft beam at similar incidence angle. It is induced by an underflow problem of the onboard analog to digital converter. As a result, mid-beam measurements for light winds are higher than they should be. The problem mainly occurs in the region for which backscatter values are low, i.e., at high incidence angles. This undesired existence of the asymmetry of the mid beam could in principle be partly corrected for by renormalizing the mid beam backscatter before it is presented to the inversion algorithm. This possibility was not explored. The underflow problem emerged from almost all methods and tools that were used in this work. Only for the ocean calibration its signature is weak. Investigation of alternative periods showed that the underflow problem was even worse in December 1997, 1999 and 2000.

In wind space, inverted CMOD5 winds are nearly unbiased when compared to the FGAT winds for the optimization period. This is true for all nodes and nearly all wind speeds. Therefore, the large negative biases of CMOD4 and the large node-dependency of the bias levels of CMOD4 and CMOD5(KNMI) have been removed. Standard deviations of CMOD5 winds relative to the FGAT winds are comparable or better than those for CMOD4 and CMOD5(KNMI). The scatter index is best for CMOD5 for all incidence angles.

The recent experimental work of Donnely *et al.* 1999, Carswell *et al.* 1999 allowed for a realistic derivation of a model function at strong wind speeds. As a result, both CMOD5(KNMI) and CMOD5 give a better representation for extreme situations. For the period between August-December 1998, winds up to 34 $\mathrm{m\,s^{-1}}$ were retrieved. The directional flow-structure of the CMOD5 winds looks for tropical cyclones more continuous than it does for CMOD4 and CMOD5(KNMI). It is likely to be the result of an improvement of the $B1$ term.

The performance of CMOD5 was also tested for the periods of the month December of 1997, 1998 (which is part of the optimization period), 1999 and 2000. Trends in the bias levels of the CMOD winds compared to such FGAT winds were shown to arise from trends in the FGAT winds. The question thus emerges, whether the FGAT winds during the optimization period were unbiased w.r.t. to 'true' winds or not. Such an answer could only be achieved by a comparison with an independent, unbiased data set (height-corrected buoy measurements are a candidate). Such a collocation study was beyond the scope of this work. The variations in bias levels between December 1997 and December 2000 were within 0.35 $\mathrm{m\,s^{-1}}$. For December 1998, CMOD5 winds were on average 0.09 $\mathrm{m\,s^{-1}}$ higher than the FGAT winds, for December 2000 they were 0.20 $\mathrm{m\,s^{-1}}$ lower than these model winds. The inter-node dependent variation of the bias (being small) and standard deviation was found to be very similar for all considered periods. Also the scatter index of CMOD5 was consistently the lowest one. Its indicates that the internal consistency and performance of CMOD5 is constant in time. A possible bias of CMOD5 winds compared to the 'truth', can probably easily be removed by updating the first four CMOD5 coefficients by multiplication with the same factor, since these coefficients set the overall backscatter level as function of wind speed.

Acknowledgments

The work presented in this paper was funded by ESRIN (Project Ref. 15988/02/I-LG). I am grateful for the helpful discussions I had with Ad Stoffelen, Siebren de Haan, Lars Isaksen, Jean Bidlot and Peter Janssen. In addition, I would like to thank Ad Stoffelen, Peter Janssen and Lars Isaksen for the detailed proofreading of this document.

Appendix: The CMOD5 model formulation and coefficients

The form of the ECMWF CMOD5 model is:

$$\sigma^0 = b_0\,(1 + b_1\cos\phi + b_2\cos 2\phi)^{1.6}, \tag{23}$$

where b_0, b_1 and b_2 are functions of wind speed v and incidence angle θ, or alternatively, $x = (\theta - 40)/25$.

The b_0 term is defined as:

$$b_0 = 10^{a_0 + a_1 v}\, f(a_2 v, s_0)^{\gamma}, \tag{24}$$

where

$$f(s, s_0) = \begin{cases} (s/s_0)^{\alpha} g(s_0) & , \quad s < s_0 \\ g(s) & , \quad s \geq s_0 \end{cases} \tag{25}$$

where

$$g(s) = 1/(1 + \exp(-s)), \quad \text{and} \quad \alpha = x_0(1 - g(s_0)) \tag{26}$$

The functions a_0, a_1, a_2, γ and s_0 depend on incidence angle only:

$$\begin{array}{rcccccc} a_0 & = & c_1 & + & c_2 x & + & c_3 x^2 \quad + \quad c_4 x^3 \\ a_1 & = & c_5 & + & c_6 x & & \\ a_2 & = & c_7 & + & c_8 x & & \\ & & & & & & \\ \gamma & = & c_9 & + & c_{10} x & + & c_{11} x^2 \\ s_0 & = & c_{12} & + & c_{13} x & & \end{array} \tag{27}$$

The $B1$ term is modeled as follows:

$$B1 = \frac{c_{14}(1 + x) - c_{15} v\,(0.5 + x - \tanh[4(x + c_{16} + c_{17} v)])}{1 + \exp(0.34(v - c_{18}))} \tag{28}$$

The b_2 term was chosen as:

$$b_2 = (-d_1 + d_2 v_2)\exp(-v_2) \tag{29}$$

Here v_2 is given by:

$$v_2 = \begin{cases} a + b(y-1)^n & , \quad y < y_0 \\ y & , \quad y \geq y_0 \end{cases} \quad , \quad y = \frac{v + v_0}{v_0} \tag{30}$$

where

$$y_0 = c_{19} \quad , \quad n = c_{20} \tag{31}$$

$$a = y_0 - (y_0 - 1)/n \quad , \quad b = 1/[n(y_0 - 1)^{n-1}]. \tag{32}$$

The quantities v_0, d_1 and d_2 are functions of incidence angle only:

$$\begin{array}{rcccccc} v_0 & = & c_{21} & + & c_{22} x & + & c_{23} x^2 \\ d_1 & = & c_{24} & + & c_{25} x & + & c_{26} x^2 \\ d_2 & = & c_{27} & + & c_{28} x & & \end{array} \tag{33}$$

The coefficients are given in Table 1, and a concise version of the CMOD5 Fortran implementation is shown in Figure 38.

```
      FUNCTION CMOD5(V,D,THDEG,AZM)
C     HANS HERSBACH  JUNE 2002  ECMWF
      PARAMETER (DTOR =57.29577951,THETM=40.,THETHR=25.,ZPOW=1.6)
      LOGICAL LFIRST /.TRUE./
      REAL            C(28),Y0,A,B,PN
      SAVE    LFIRST, C    ,Y0,A,B,PN
      IF (LFIRST) THEN
          LFIRST=.FALSE.
          OPEN(510) ; READ(510,*)C ; CLOSE(510)
          Y0=C(19)  ; PN=C(20)
          A = Y0-(Y0-1.)/PN
          B = 1./(PN*(Y0-1.)**(PN-1.))
      ENDIF
      CSFI  = COS((D - AZM)/DTOR)
      X     = (THDEG - THETM) / THETHR  ; XX = X*X
      A0    = C( 1)+C( 2)*X+C( 3)*XX+C( 4)*X*XX
      A1    = C( 5)+C( 6)*X
      A2    = C( 7)+C( 8)*X
      GAM   = C( 9)+C(10)*X+C(11)*XX
      S0    = C(12)+C(13)*X
      S     = A2*V
      A3    = 1./(1.+EXP(-MAX(S,S0)))
      IF      ( S.LT.S0) A3 = A3*(S/S0)**(S0*(1.-A3))
      B0    = (A3**GAM)*10.**(A0+A1*V)
      B1    = C(15)*V*(0.5+X-TANH(4.*(X+C(16)+C(17)*V)))
      B1    = (C(14)*(1.+X)-B1)/(EXP( 0.34*(V-C(18)) )+1.)
      V0    = C(21) + C(22)*X + C(23)*XX
      D1    = C(24) + C(25)*X + C(26)*XX
      D2    = C(27) + C(28)*X
      V2    = (V/V0+1.)
      IF      (V2.LT.Y0) V2 = A+B*(V2-1.)**PN
      B2    = (-D1+D2*V2)*EXP(-V2)
      CMOD5 = B0*(1.0+B1*CSFI+B2*(2.*CSFI*CSFI-1.))**ZPOW
      END
```

Figure 38: The concise version of the CMOD5 code

Parameter	Coefficient	Value	Parameter	Coefficient	Value
a_0	c_1	-0.688		c_{15}	0.007
	c_2	-0.793		c_{16}	0.33
	c_3	0.338		c_{17}	0.012
	c_4	-0.173		c_{18}	22.0
a_1	c_5	0.0	y_0	c_{19}	1.95
	c_6	0.004		c_{20}	3.0
a_2	c_7	0.111	v_0	c_{21}	8.39
	c_8	0.0162		c_{22}	-3.44
γ	c_9	6.34		c_{23}	1.36
	c_{10}	2.57	d_1	c_{24}	5.35
	c_{11}	-2.18		c_{25}	1.99
s_0	c_{12}	0.4		c_{26}	0.29
	c_{13}	-0.6	d_2	c_{27}	3.80
b_1	c_{14}	0.045		c_{28}	1.53

Table 1: The CMOD5 coefficients

References

Attema, E., P., W., (1986). An experimental campaign for the determination of the radar signature of the ocean at C-band. *Proc. Third International Colloquium on Spectral Signatures of Objects in Remote Sensing*, Les Arcs, France, ESA, **SP-247**, 791-799.

Carswell, J. R., Castells A., Knapp E. J., Chang P. S., Black P. G. and F. Marks, (1999). Observed Saturation in in C and Ku-band Ocean Backscatter at Hurricane Force Winds. *unpublished*.

Cavanié, A., and D. Offiler, (1986). ERS-1 wind scatterometer: wind extraction and ambiguity removal. *Proc. IGARSS 1986; Todays Solutions for Tomorrows Information Needs*, Zurich, Switzerland, ESA **SP-254**, 395-398.

Donnelly, W. J., Carswell J. R., McIntosh R. E., Chang P. S., Wilkerson J., Marks F., and P. G. Black (1999). Revised Ocean Backscatter Models at C and Ku-band under High-wind Conditions, *J. Geophys. Res.*, **104** (C5) 11,485-11,497.

Francis, R, Graf G., Edwards P. G., McCaig M., McCarthy C., Dubock P., Lefebvre A., Pieper B., Pouvreau P, Y., Wall R., Wechsler F., Louet J., and R. Zobl. (1991) The ERS-1 spacecraft and its payload. *ESA Bulletin*, (65):27–48, Feb. 1991. ERS-1 Special Issue.

Gérard, É, and T. McNally (1999). Assimilation of SSMI/1D-Var 10-metre wind speed, *Memorandum Research Department*, **R43/EG/73**, ECMWF, Reading, England.

Haan, de, S and A. C. M. Stoffelen, (2001). CMOD5, **SAF/OSI/KNMI/TEC/TN/140**, www.eumetsat.de/en/area4/saf/internet/other_reports/SAFOSI_W_cmod5-knmi.pdf, EUMETSAT-Publications Division, EUMETSAT, Darmstadt, Germany.

Isaksen, L, (1997). Impact of ERS scatterometer data in the ECMWF 4D-Var assimilation system. Preliminary studies. In *Space at the Service of our Environment*, 1,829-1,851, Florence, Italy, May 1997, ESTEC, European Space Agency [SP-414]. Available from ESA Publications Division, ESTEC Noordwijk, The Netherlands.

Isaksen, L. and A. C. M. Stoffelen, (2000). ERS scatterometer wind data impact on ECMWF's tropical

cyclone forecasts. *IEEE Trans. Geosci. Remote Sens.*, **38** (4), 1,885-1,892.

Janssen, P. A. E. M, Wallbrink H., Calkoen, C. J., Halsema, van D., Oost, W. A. and P. Snoeij, (1998) VIERS-1 scatterometer model. *J. Geophys. Res.*, **103** (C4) 7,807-7,831.

Janssen, P. A. E. M, Doyle J. D., Bidlot J., Hansen B., Isaksen L., and P. Viterbo (2000) Impact and feedback of ocean waves on the atmosphere. *Advances in Fluid Mechanics, Atmosphere-Ocean Interactions,* Vol. **I**, WITpress, Ed. W. Perrie, 155-197.

Leidner, S. M, Isaksen, L, and R. N. Hoffman, (2003) Impact of NSCAT winds on tropical cyclones in the ECMWF 4D-Var assimilation system, *Mon. Wea. Rev.*, **131,** 3-26.

LeMeur, D., Isaksen L., Stoffelen A. (1997). Wind Calibration by Triple Collocation and Maximum Likelihood Estimation. In Proc. of *The CEOS Wind and Wave Validation Workshop*, Noordwijk, 3-5 June 1997, ESA WPP-147, ESA-Publications Division, ESTEC, Noordwijk (NL).

Rabier, F., H. Järvinen, E. Klinker, J.F. Mahfouf and A. Simmons (2000). The ECMWF operational implementation of four-dimensional variational assimilation. Part I: experimental results with simplified physics. *Q. J. R. Meteorol. Soc.* **126**, 1143-1170.

Offiler, D., (1994). The Calibration of ERS-1 Satellite Scatterometer Winds, *J. Atmos. Oceanic Technol.*, **11,** 1,002-1,017.

Stoffelen, A. C. M., (1998). Error modeling and calibration; towards the true surface wind speed, *J. Geophys. Res.*, **103,** (C4) 7,755-7,766.

Stoffelen, A. C. M., (1999). A simple method for calibration of a scatterometer over the ocean, *J. Atmos. Oceanic Technol.*, **16,** 275-282.

Stoffelen, A. C. M., and D. L. T. Anderson, (1997a). Scatterometer Data Interpretation: Measurement Space and Inversion, *J. Atmos. Oceanic Technol.*, **14,** 1,298-1,313.

Stoffelen, A. C. M., and D. L. T. Anderson, (1997b). Scatterometer Data Interpretation: Derivation of the Transfer Function CMOD4, *J. Geophys. Res.*, **102** (C3) 5,767-5,780.

Stoffelen, A. C. M., and D. L. T. Anderson, (1997c). Ambiguity removal and assimilation of scatterometer data. *Quart. J. Roy. Meteor. Soc.* **123,** 491-518.

Stoffelen, A. C. M., (2000). A generic approach for assimilating scatterometer observations. In *Exploration of the New Generation of Satellite Instruments for Numerical Weather Prediction, Seminar proceedings*, 73-99.

Teixeira, J. (1999) The impact of increased boundary layer vertical resolution on the ECMWF forecast system. *ECMWF Technical memorandum* **268**, ECMWF, Reading, England.

Tomassini, M., LeMeur D., and R. W. Saunders, (1998) Near-surface satellite wind observations of hurricanes and their impact on ECMWF model analysis and forecasts, *Mon. Wea. Rev.*, **126,** 1,274-1,286.

Wentz, F. J and D. K. Smith (1999) A model function for the ocean-normalized radar cross section at 14 GHz derived from NSCAT observations, *J. Geophys. Res.*, **104** (C5) 11,499-11,514.